

Higher-derivative four-dimensional sine-Gordon model

Matteo F. Bontorno

*Dipartimento di Fisica e Astronomia “Ettore Majorana”,
Università di Catania, 64, Via S. Sofia, I-95123 Catania, Italy;
Scuola Superiore di Catania, Università di Catania, 9, Via Valdisavoia, I-95123 Catania, Italy; and
Centro Siciliano di Fisica Nucleare e Struttura della Materia, Catania, Italy.*

G.G.N. Angilella

*Dipartimento di Fisica e Astronomia “Ettore Majorana”,
Università di Catania, 64, Via S. Sofia, I-95123 Catania, Italy;
Scuola Superiore di Catania, Università di Catania, 9, Via Valdisavoia, I-95123 Catania, Italy;
INFN, Sezione di Catania, Via Santa Sofia 64, 95123 Catania, Italy. and
Centro Siciliano di Fisica Nucleare e Struttura della Materia, Catania, Italy.*

Dario Zappalà

*INFN, Sezione di Catania, Via Santa Sofia 64, 95123 Catania, Italy; and
Centro Siciliano di Fisica Nucleare e Struttura della Materia, Catania, Italy.*

ABSTRACT

The phase structure of a higher derivative sine-Gordon model in four dimensions is analysed. It is shown that the inclusion of a relevant two-derivative term in the action significantly modifies some of the results obtained by neglecting this operator, and the final picture is substantially different from the one describing the phase diagram associated with the two-dimensional Berezinskii-Kosterlitz-Thouless (BKT) transition. The study is carried out with the help of the Renormalization Group (RG) flow equations, determined for a set of three parameters, and numerically solved both for a truncated series expansion approximation, and for the complete set of equations. In both cases, a continuous line of fixed points, terminating at a particular point presenting universal properties, is found, together with a manifold that separates two phases, roughly characterized by the sign of the coupling \tilde{z}_k associated with this newly included operator. While the phase corresponding to $\tilde{z}_k > 0$ shows some pathologies, the one with $\tilde{z}_k < 0$ has a well-behaved infrared limit, where the system reduces to a Gaussian-like model. We also briefly comment about the possibility that our model could capture some of the qualitative features of the ultraviolet (UV) critical manifold of conformally reduced gravity.

I. INTRODUCTION

Field theories containing higher derivative kinetic terms have received long-standing attention, as they present the remarkable advantage of an improved ultraviolet (UV) regime due to the smoothening of loop integrals in the high loop momentum limit, because of the higher powers of momentum in the propagators. Therefore, various applications have been considered so far to theories that are otherwise non-renormalizable, such as the case of the field theoretical formulation of gravity [1–6].

Actually, this approach suffers from a fundamental inconvenience, as theories that contain more than two time derivatives are affected by the Ostrogradski instability, associated with the violation of unitarity [4, 7]. This means that higher derivative theories containing the same number of space and time derivatives, a property that is essential to comply with Lorentz symmetry, unavoidably must bear with the violation of other basic principles which are characteristic of a fundamental theory.

In this sense, field theories with an anisotropic structure, i.e. with actions containing two derivatives with respect to the time coordinate, but 2τ derivatives with respect to the space coordinates (τ is usually indicated as the anisotropy exponent), have been analysed. So, for instance, the Hořava-Lifshitz gravity [8, 9] is a renormalizable anisotropic gravitational theory, constructed on the basis of these motivations (for a more recent version of this formulation see Refs. [10–13]). In addition, anisotropic field theories on flat spacetime were also formulated on the same grounds [14–24]. Clearly, this class of actions does not fulfill Lorentz symmetry, that can eventually be recovered at low energy as an emergent property, but it is essential to require that the related theoretical predictions are not in contradiction with the observational constraints [25, 26].

However, the study of isotropic higher derivative theories, i.e. with actions containing the same number of space and time derivatives, has nevertheless been pursued, because they can still be regarded as effective field theories, possibly generated by some integration of more fundamental degrees of freedom and, therefore, not necessarily constrained by all fundamental principles, that are still helpful as examples of renormalizable theories. In addition, the relevance of these isotropic, higher derivative theories also comes from the fact that, when Wick-rotated, they acquire the usual physical interpretation of a statistical model in a d -dimensional space.

The renormalization of these higher-derivative theories is regulated by the presence of a particular class of fixed points, called Lifshitz points, that may show up in both isotropic and anisotropic actions [27]. Concerning statistical systems, they are typically associated to the existence of tricritical points in the phase diagram, which signal the coexistence of three phases, including one that presents a non-uniform, modulated ground state. This has several realisations in condensed matter, such as magnetic systems, but also polymer mixtures, liquid crystals, high-Tc superconductors (for reviews on this subject see [28–31]), as well as in the analysis of dense quark matter with the realization of unconventional phases [32–36].

From the point of view of renormalization, the appearance of Lifshitz points comes from a change of the scaling dimensions of the various couplings in the action with respect to the canonical dimensions, due to the presence of a higher derivative term which set the new scaling dimension of the field, different from its canonical dimension determined instead by the two derivative kinetic term. The change of scaling dimensions modifies the nature of the Renormalization Group (RG) flow equations and the structure of fixed points that regulate the renormalization properties of the theory [27].

In the past years, this modification of the scaling dimension was exploited in a series of papers [37–39], to establish a relation between the four-dimensional (4D) isotropic higher-derivative scalar theories, characterized by the kinetic term $W \partial^2 \phi \partial^2 \phi$, and the two-dimensional (2D) standard theory with kinetic term $Z \partial \phi \partial \phi$, as both models, in the presence of a continuous internal symmetry $O(N)$, show typical features of systems defined in a \bar{d} -dimensional space, \bar{d} being equal to their lower critical dimension.

The non-perturbative approach used in this investigation is the RG analysis, based on the Functional RG flow equations [40–42], which, for instance, was extensively used to produce a comprehensive picture of the universal properties of $O(N)$ field theories as a function of the dimension d and the index N [43–45], as well as of topological phase transitions such as the 2D Berezinskii - Kosterlitz - Thouless (BKT) transition [46–50] and of the sine-Gordon model [51–56], that belongs to the same universality class.

Then, in [57, 58], the RG technique developed for the 2D topological transitions, was exported to 4D systems, by first mapping an $O(2)$ -symmetric four-derivative model onto a higher derivative sine-Gordon model (analogous to the well established mapping between the XY and the sine-Gordon model in 2D [59]), and then studying the RG flow equations obtained for the latter. The picture emerging from this analysis remarkably shows several features of the BKT universality class [60–63], such as the presence

of a line of fixed points terminating at an end point associated with a universal value of the anomalous dimension η .

In this paper, we plan to further investigate this issue, as in [58] it was pointed out that, when passing from a 2D to a 4D system, a few relevant differences appear, besides the mentioned similarities. In fact, the 4D sine-Gordon model RG flow equations present a sign flip with respect to the 2D case, that unavoidably modifies the phase diagram. Here, we reconsider the analysis of [58] and, besides deriving the flow equation within a different approach to provide an additional check of the change of sign in the RG equations, we enlarge our model, by including an additional two-derivative kinetic term into the 4D sine-Gordon model, which was previously neglected, in order to get a more comprehensive description of such a universality class. Actually, the inclusion of such a term is a crucial point, as it turns out to be a relevant operator, according to the computation of its scaling dimension and, consequently, it plays an essential role in determining the actual infrared (IR) limit of the RG flow and the complete structure of the phase diagram.

In Sec. II, we introduce the specific model and the associated complete RG flow equations. We also summarise the results obtained in the approximation studied in [58], to better clarify the improvements achieved in this paper. Sec. III is devoted to the results of a truncated version of the RG flow equations (after an expansion in powers of the couplings around the line of fixed points), which is simpler to handle but sufficient to grasp the main features of our model. In Sec. IV the results derived from the full RG equation are investigated. Then, in Sec. V we discuss the possible future perspectives of the present analysis. Finally, Appendix A contains the main details of the derivation of the RG flow equations, while in Appendix B an alternative derivation of the RG equations, based on a perturbative approach, is presented.

II. GENERALIZED SINE-GORDON MODEL

In the following we shall discuss the phase structure of the Euclidean 4D model defined by ($\Delta \equiv \partial_\mu \partial_\mu$)

$$S[\Phi] = \int d^4x \left[\frac{w}{2} \Delta \Phi(x) \Delta \Phi(x) + \frac{Z}{2} \partial_\mu \Phi(x) \partial_\mu \Phi(x) + g(1 - \cos \beta \Phi) \right] \quad (1)$$

which generalizes the sine-Gordon model discussed in [58], where the two-derivative term is absent by imposing $Z = 0$. In Eq. (1), the parameter β is included to keep the product $\beta \Phi$ adimensional, whatever the engineering dimension of the field Φ . Clearly one can get rid of β , by replacing in Eq. (1) :

$$u = w/\beta^2 \quad ; \quad z = Z/\beta^2 \quad ; \quad \varphi = \beta \Phi . \quad (2)$$

Then, the actual value of β can be absorbed in the scale of the Lagrangian, which forms the argument of the integral defining the action in Eq. (1). A similar situation occurs when considering a simple model for the degenerate electron gas, including the electronic kinetic energy and Coulomb repulsion, as well as a uniform positive background, where all lengths and wavevectors are scaled using the Wigner radius r_s . In that case, the overall Hamiltonian acquires a factor of $1/r_s^2$, while the (renormalized) interaction term exhibits a relative scale of r_s with respect to the kinetic energy term (see e.g. Eq. (3.24) of [64]).

However, for the specific case in Eq. (1), β is to be regarded as a fixed external parameter that does not get modified by the RG transformations along the flow, as stated in [56]. This, in turn, means that, once the redefinitions (2) are inserted in Eq. (1), any other rescaling of the field does imply a genuine physical scale change in the model. In fact, in the usual 2D sine-Gordon model, different values of the field renormalization (i.e. the coefficient of the term containing two derivatives of the field), produce physically distinct fixed points of the system unlike, for instance, the critical exponents of the 3D Wilson-Fisher fixed point that are not modified by a global rescaling of the field renormalization, which is compensated by an unobservable redefinition of the field, as shown, e.g., in [65].

The model with $Z = 0$ analysed in [58], shows many features that are characteristic of the 2D BKT transition, namely the presence of a line of fixed points parametrized by a variable which undergoes a universal jump from a finite value to zero, at a specific critical point. Unfortunately, other details, and in particular the full phase diagram, of the BKT transition were not recovered in [58], because of the differences in the flow equations obtained in that particular case with respect to those governing the 2D BKT transition. Hence, after deriving the flow equations for the model (1) we shall reconsider the case with $Z = 0$, analyzing in detail its flow.

The study of the phase structure of our model can be performed by means of the Functional Renormalization Group (RG), where the effect of fluctuations is represented in terms of a functional differential flow equation which describes the evolution with a momentum scale k of the various parameters of the average effective action functional, defined in accordance with Eqs. (1) and (2)

$$\Gamma_k[\varphi] = \int d^d x \left[\frac{u_k}{2} \partial^2 \varphi \partial^2 \varphi + \frac{z_k}{2} \partial_\mu \varphi \partial_\mu \varphi + g_k (1 - \cos \varphi) \right] \quad (3)$$

where, without loss of generality, we eliminated the parameter β by making use of the replacements displayed in Eq. (2) (but we shall come back to the original form in Eq. (1) at the end of Sec. IV to discuss the IR limit of the model). We also generalised Eq. (3) to d dimensions. This is done for computational convenience, as discussed in Appendix A, and the limit $d \rightarrow 4^+$ is taken only as the last step of our calculation. Then, the parameters, u_k , z_k , g_k in (3) show a new dependence on the energy scale k , as we let them evolve according to a set of RG differential equations, starting from a set of values assigned to the microscopic model at the UV scale $k = \Lambda$, down to the IR region for $k \rightarrow 0$. In particular, we shall resort to the RG flow equation [42]

$$\partial_t \Gamma_k[\varphi] = \frac{1}{2} \text{Tr} \frac{\partial_t R_k}{\Gamma_k^{(2)}[\varphi] + R_k} \quad (4)$$

with $t = \log(\Lambda/k)$, and the trace is taken over spatial and momentum degrees of freedom; $\Gamma_k^{(2)}[\varphi]$ is the second functional derivative of $\Gamma_k[\varphi]$ with respect to the field φ ; finally R_k is the scale dependent regulator function which effectively generates the progressive integration of the UV modes along the flow. For our purposes, it is sufficient to select the simple form [58]

$$R_k = k^4. \quad (5)$$

Then, one has to suitably project the full flow equation (4), in order to determine the flow of the three parameters u_k , z_k , g_k . In particular, the projection on x -independent field configurations selects the flow equation for the potential $V_k(\varphi) = \int d^d x g_k (1 - \cos \varphi)$

$$\partial_t V_k(\varphi) = \frac{1}{2} \int \frac{d^d q}{(2\pi)^d} (\partial_t R_k) G_k(q), \quad (6)$$

where

$$G_k(q) = \left(\Gamma_k^{(2)} + R_k \right)^{-1}, \quad (7)$$

and $V_k''(\varphi)$ is the second derivative of the potential with respect to φ . In order to determine the flow of g_k , it is sufficient to select the coefficient of $\cos \varphi$, which is realised by applying on both sides of Eq. (6) the projector [58]:

$$P_1 = -\frac{1}{\pi} \int_{-\pi}^{\pi} d\varphi \cos \varphi. \quad (8)$$

On the other hand, the determination of the flow equations for the coefficients of the derivatives of the field, namely u_k and z_k , requires one more step. In fact, one has first to determine the flow of the two-point function $\Gamma_k^{(2)}[\varphi]$ by differenziating Eq. (4) twice with respect to the field φ :

$$\begin{aligned} \partial_t \Gamma_k^{(2)}(-p, p, \varphi) = \\ \int \frac{d^d q}{(2\pi)^d} \frac{(\partial_t R_k)}{2} \left[2 \frac{\Gamma_k^{(3)}(p, q, p-q, \varphi)}{\Gamma_k^{(2)}(-q, q, \varphi) + R_k} G_k(p+q) \frac{\Gamma_k^{(3)}(p, p+q, -q, \varphi)}{\Gamma_k^{(2)}(-q, q, \varphi) + R_k} - \frac{\Gamma_k^{(4)}(p, q, -q, -p)}{(\Gamma_k^{(2)}(-q, q, \varphi) + R_k)^2} \right], \end{aligned} \quad (9)$$

where we explicitly displayed the dependence on the specific momenta, of the two-, three-, four-field derivatives of the average action: $\Gamma_k^{(2)}$, $\Gamma_k^{(3)}$, $\Gamma_k^{(4)}$. However, according to the ansatz in Eq. (3), in the following we shall compute the n -point functions in Eq. (9), as the n -derivative of the action in (3). In

this approximation, $\Gamma_k^{(3)}$ and $\Gamma_k^{(4)}$ are identified with the third and fourth derivatives of the potential $V_k(\varphi)$, respectively, and do not carry any dependence on the external momentum p of Eq. (9), while, according to the definition in Eq. (7), for the two-point function we have

$$G_k(q) = \frac{1}{u_k q^4 + z_k q^2 + V_k''(\varphi) + R_k} . \quad (10)$$

The flow equations for u_k (or z_k) are obtained by taking four (two) derivatives with respect to the external momentum p and then applying on both sides of Eq. (9) the projector

$$P_0 = \frac{1}{2\pi} \int_0^{2\pi} d\varphi \quad (11)$$

which yields

$$\partial_t u_k = \frac{P_0}{4!} \lim_{p \rightarrow 0} \int \frac{d^d q}{(2\pi)^d} \partial_t R_k G(q)^2 V_k^{(3)}(\varphi)^2 \frac{d^4}{dp^4} G(p+q) \quad (12)$$

$$\partial_t z_k = \frac{P_0}{2!} \lim_{p \rightarrow 0} \int \frac{d^d q}{(2\pi)^d} \partial_t R_k G(q)^2 V_k^{(3)}(\varphi)^2 \frac{d^2}{dp^2} G(p+q) . \quad (13)$$

Note that the last term on the right hand side of Eq. (9), proportional to $\Gamma_k^{(4)}$, does not contribute to Eqs. (12), (13), because in our scheme it has no dependence on the external momentum p .

Of course, the significant RG flow is obtained for the variables suitably expressed in units of the running scale k . In our case, we expect the non-perturbative dynamics to be driven by the higher derivative term in Eq. (3). This, in turn, means that the coefficient of the higher derivative term, u_k has zero scaling dimension, and consequently also the field φ has zero scaling dimension. Then, after a simple dimensional analysis, we define the new (scaling) dimensionless variables

$$\tilde{z}_k \equiv \frac{z_k}{k^2} \quad ; \quad \tilde{g}_k \equiv \frac{g_k}{k^4} \quad (14)$$

while, since $\tilde{u}_k = u_k$, in this case we do not change notation and keep the dimensionless variable u_k . This redefinition of the scaling dimensions, different from the usual case where the coefficient of the two-derivative term z_k is taken as dimensionless, leads to the presence of Lifshitz points, and a peculiar UV structure even for the simplified version of model (1), where the two derivative term is omitted [58], and here we analyse the case where z_k is turned on.

The RG calculation yields the three beta-functions

$$\begin{aligned} \partial_t u_k &= \beta_u(u_k, \tilde{z}_k, \tilde{g}_k) \\ \partial_t \tilde{z}_k &= \beta_z(u_k, \tilde{z}_k, \tilde{g}_k) \\ \partial_t \tilde{g}_k &= \beta_g(u_k, \tilde{z}_k, \tilde{g}_k) . \end{aligned} \quad (15)$$

Details of the computation are provided in Appendix A and the explicit form of $\beta_u(u_k, \tilde{z}_k, \tilde{g}_k)$, $\beta_z(u_k, \tilde{z}_k, \tilde{g}_k)$ and $\beta_g(u_k, \tilde{z}_k, \tilde{g}_k)$ is given respectively in Eqs. (A11), (A16), (A19).

Before considering the complete problem of three coupled equations, let us summarize the main features of the case where the two derivative term is omitted, i.e. $z_k = 0$ is kept fixed while focussing on the flow of u_k and \tilde{g}_k only. If one sets $z_k = 0$ in (A11), (A19), the corresponding equations are significantly simplified and they coincide with those derived in [58]:

$$\partial_t u_k = - \frac{\tilde{g}_k^2}{160\pi^2 \sqrt{(1 - \tilde{g}_k^2)^3}} \quad (16)$$

$$\partial_t \tilde{g}_k = 4\tilde{g}_k - \frac{1}{8\pi^2 u_k \tilde{g}_k} \left(1 - \sqrt{1 - \tilde{g}_k^2} \right) . \quad (17)$$

It should be noted however that the constraint $\tilde{z}_k = 0$ does not imply $\partial_t \tilde{z}_k = 0$, and we shall come back to this point in Sec. III.

Eqs. (16) and (17) are extremely similar to those of the two-dimensional sine-Gordon model with the coupling u_k associated to the two-derivative term (and with the four-derivative term neglected). The essential qualitative difference is the negative sign of the right hand side of Eq. (16) which is instead positive in the two-dimensional case; conversely, Eq. (17) has the same structure in both cases.

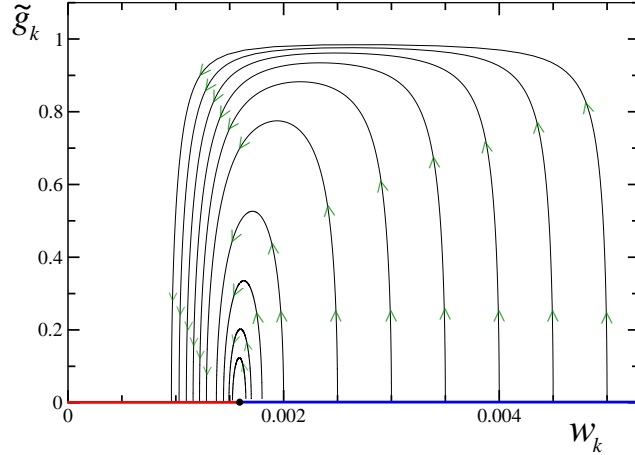


FIG. 1: Structure of the flow associated to Eqs. (16) and (17). $\tilde{g}_k = 0$ is a fixed point line, with (blue online) repulsive points above $u_k^* = 1/(64\pi^2)$ and (red) attractive points below u_k^* .

As a consequence, the two and four-dimensional Sine Gordon model share the same properties on the $\tilde{g}_k = 0$ line, as it can be checked by first expanding Eq. (17) for small $\tilde{g}_k \simeq 0$, and then taking the limit $\tilde{g}_k \rightarrow 0$. In this limit one finds $\partial_t \tilde{g}_k \rightarrow 0^+$ and $\partial_t \tilde{g}_k \rightarrow 0^-$ respectively for $u_k > 1/(64\pi^2)$ and $u_k < 1/(64\pi^2)$, and in both cases $\partial_t u_k = 0$. Then one concludes that $\tilde{g}_k = 0$ is a line of fixed points for the coupled equations (16) and (17), that are repulsive or attractive (when the scale flows toward the IR $k \rightarrow 0$), respectively above and below the point

$$u_k^* = \frac{1}{64\pi^2}. \quad (18)$$

The differences between the two and four-dimensional Sine Gordon model arise when $\tilde{g}_k \neq 0$, because of the opposite sign in Eq. (16). In fact, for the two-dimensional case the positive sign produces the well known BKT phase structure with one phase characterised by the IR attractive fixed points below u_k^* separated by the other phase which is instead dominated by the repulsive fixed points above u_k^* . In this case the negative sign forces u_k to decrease whenever $\tilde{g}_k \neq 0$ and in Fig. 1 the structure of the flow generated by Eqs. (16) and (17) is shown. As expected, all lines terminate at one IR fixed point with $u_k < u_k^*$ and $\tilde{g}_k = 0$, on the red segment. Points with $u_k > u_k^*$ and $\tilde{g}_k = 0$, are unstable fixed points. However, for $\tilde{g}_k \neq 0$, the flow in Fig. 1 is uniform and no line separating different regions of the diagram, i.e. no phase structure is present: the system shows only one phase on the plane $(u_k - \tilde{g}_k)$.

As a double check of this neat difference with respect to the two-dimensional case, in Appendix B we derive the flow equations by following a perturbative approach developed in [63] for the two dimensional Coulomb gas. In fact, it turns out that the negative sign in Eq. (16) is due to the specific number of dimensions, $d = 4$, analysed in this case. Nevertheless, the above picture is not complete, as we have totally neglected the effect of the relevant coupling \tilde{z} so far. In the next two Sections we show the important role of \tilde{z} in establishing the phase structure of model (1).

III. TRUNCATED FLOW EQUATIONS

Instead of tackling the full flow in Eqs. (15), we start by considering a simplified problem where the differential equations are studied around the axis $\tilde{g}_k = \tilde{z}_k = 0$ which, as we will see, is still a line of fixed points, and therefore we expand the right-hand side of Eqs. (15) in powers of \tilde{g}_k and \tilde{z}_k and retain terms at most quadratic in the product of these two parameters. The output of the expansion is:

$$\partial_t u_k = -\frac{\tilde{g}_k^2}{160\pi^2} \quad (19a)$$

$$\partial_t \tilde{z}_k = 2\tilde{z}_k + \frac{3}{512\pi\sqrt{u_k}}\tilde{g}_k^2 \quad (19b)$$

$$\partial_t \tilde{g}_k = \left(4 - \frac{1}{16\pi^2 u_k}\right)\tilde{g}_k + \frac{\tilde{g}_k \tilde{z}_k}{64\pi u_k^{3/2}} \quad (19c)$$

First we notice that Eqs. (19) are invariant under the transformation $\tilde{g}_k \rightarrow -\tilde{g}_k$ and therefore the findings with $\tilde{g}_k > 0$, discussed below, hold also if the sign of the coupling \tilde{g}_k is flipped. Then, a direct analysis of the zeroes of the truncated differential equations, shows that the only fixed points solutions of Eqs. (19) are, as already anticipated, all the points of the axis $\tilde{g}_k = \tilde{z}_k = 0$ (we focus only on positive $u_k > 0$, in order to have a stable model). On the other hand, a direct inspection of Eq. (19c) shows that the point u_k^* in Eq. (18) still represents the critical point that marks the different nature of the fixed points for $u_k < u_k^*$ or $u_k > u_k^*$. In fact \tilde{z}_k is clearly a relevant coupling as evident from Eq. (19b), then, for $u_k > u_k^*$, all points on this axis are repulsive fixed points all trajectories flow away from them, while for $u_k < u_k^*$, unlike the diagram in Fig. 1 there is one new relevant direction associated to \tilde{z}_k and the points are no longer IR stable.

Therefore, one concludes that all points characterized by $\tilde{z}_k = 0$ and $\tilde{g}_k \neq 0$ are not fixed points: even the single Eq. (19b) has a non-vanishing right-hand side at these points, i.e. $\partial_t \tilde{z}_k \neq 0$. This means that we cannot expect to observe the flow depicted in Fig. 1 when the complete set of equations (19) is solved with initial conditions taken on the plane $\tilde{z}_k = 0$ (with $\tilde{g}_k \neq 0$), i.e. we cannot expect the plane $\tilde{z}_k = 0$ to be the manifold that separates two different phases of our model, because it is crossed by the trajectories generated by equations (19). Nevertheless, we can still check the behavior of the flow around the two manifolds defined by the two constraints $\partial_t \tilde{z}_k = 0$ and $\partial_t \tilde{g}_k = 0$.

These manifolds are plotted in Fig. 2. Namely, the surface corresponding to $\partial_t \tilde{z}_k = 0$ is the one that embeds the straight line of fixed points $\tilde{g}_k = \tilde{z}_k = 0$ (orange surface online), while the other manifold corresponds to $\partial_t \tilde{g}_k = 0$ (blue online). More precisely, in addition to the points on the latter manifold, the constraint $\partial_t \tilde{g}_k = 0$ also holds for all points on the plane $\tilde{g}_k = 0$.

The two manifolds in Fig. 2 separate four different regions: region I, where $\partial_t \tilde{z}_k < 0$, $\partial_t \tilde{g}_k < 0$; region II, where $\partial_t \tilde{z}_k > 0$, $\partial_t \tilde{g}_k < 0$; region III, where $\partial_t \tilde{z}_k < 0$, $\partial_t \tilde{g}_k > 0$; region IV, where $\partial_t \tilde{z}_k > 0$, $\partial_t \tilde{g}_k > 0$. Then, one can predict the trajectory of the flow, according to the location of the starting point.

- 1) The initial point is taken in region I. In this case \tilde{z}_k gets more and more negative and \tilde{g}_k decreases to 0 safely. Note that the possibility that the trajectory crosses the plane $\tilde{g}_k = 0$ is excluded because on this plane $\partial_t \tilde{g}_k = 0$ so the trajectory is forced to have $\tilde{g}_k > 0$.
- 2) The initial point is taken in region IV. \tilde{z}_k and \tilde{g}_k grow positive but u_k decreases until it reaches 0, which is a spinodal point as Eqs. (19b) and (19c) are singular at $u_k = 0$.
- 3) The initial point is located within region II. In this case one can distinguish two cases. In fact, either \tilde{z}_k grows positive while \tilde{g}_k decreases and the trajectory crosses the orange surface and the flow afterwards proceeds according to point 1), or, if the initial point is too far from the orange manifold the trajectory crosses the blue manifold and the conditions of point 2) are recovered. As in point 1), the trajectory cannot cross the plane $\tilde{g}_k = 0$ and therefore \tilde{g}_k remains positive until the blue manifold is eventually crossed.
- 4) The initial point is taken in region III. In this case, \tilde{g}_k grows and \tilde{z}_k diminishes so that the orange surface is crossed and region IV is entered and we are back to point 2), unless the initial point is very close to the blue manifold, so that the trajectory crosses the latter and ends up in region I, as in the case of point 1).

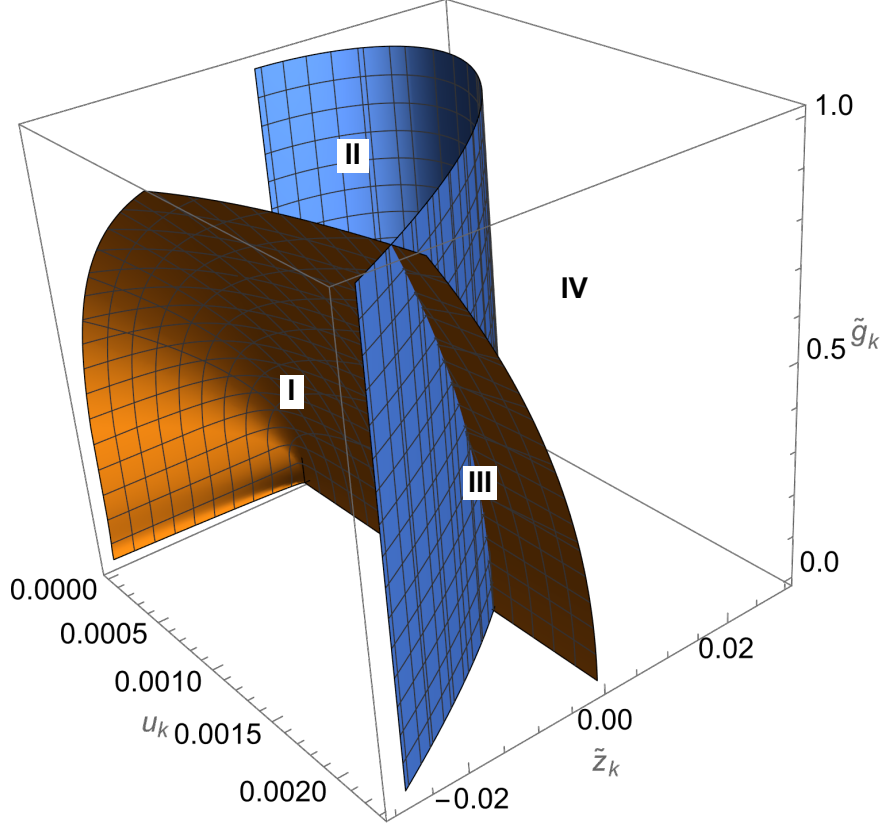


FIG. 2: Three-dimensional representation of the manifolds defined by $\partial_t \tilde{z}_k = 0$ which embeds the line of fixed points $\tilde{g}_k = \tilde{z}_k = 0$ (orange online) and $\partial_t \tilde{g}_k = 0$ (blue online). See text for the description of regions I, II, III, IV.

Finally, if the initial point is taken on the plane $\tilde{g}_k = 0$, both u_k and \tilde{g}_k remain unchanged, according to Eqs. (19), and the flow concerns \tilde{z}_k that grows to large positive (negative) values if its initial value is positive (negative). Then, in all cases the trajectories in the IR limit end either in region I or region IV.

This analysis clearly signals the presence of two phases associated to the different behavior of the trajectories in the IR limit, and one can speculate on the features of the manifold that represents the separatrix of the flows in the two phases. In fact, this manifold must contain the straight line of fixed points $\tilde{g}_k = \tilde{z}_k = 0$, and, in proximity of this line, it has to stay very close to the plane $\tilde{z}_k = 0$, although for larger \tilde{g}_k it is bent toward negative \tilde{z}_k . An initial point taken on the separatrix generates a flow totally contained within this manifold, that in the IR limit reaches a fixed point on the line with $\tilde{g}_k = \tilde{z}_k = 0$ and $u_k < u_k^*$, in a way that resembles the flow in Fig. 1, where $\tilde{z}_k = 0$ is artificially enforced.

To visualize the separation of the flows in the two phases, we show below the plots of the trajectories that start at fixed \tilde{g}_k with two slightly different values of \tilde{z}_k , located on different sides of the separatrix, thus producing flows that end either in region I or IV. Namely in Fig. 3, for nine different initial values of u_k , we choose $\tilde{g}_k = 10^{-3}$, and $\tilde{z}_k = -10^{-7}$ for one phase and $\tilde{z}_k = 0$ for the other; in Fig. 4 for the same u_k , we take $\tilde{g}_k = 10^{-1}$, and $\tilde{z}_k = -10^{-3}$ for one phase and $\tilde{z}_k = -10^{-4}$ for the other.

In both figures, we report the projection of the flow on the three coordinate planes associated with u_k , \tilde{z}_k , \tilde{g}_k . The different behavior of the flow in the two phases is evident both in the (a) and (c) plots of Figs. 3, 4. In fact, in one phase (red curves for online figures), \tilde{z}_k gets more and more negative, u_k stays constant and \tilde{g}_k , after a small bump, rapidly drops to zero. In the other phase (blue curves for online figures), \tilde{z}_k becomes positive while u_k approaches zero and, at the same time, \tilde{g}_k rapidly grows, so that the flow ends by hitting a spinodal point at $u_k = 0$. In the (b) plots the red curves with negative \tilde{z}_k of the former phase, are invisible due to the large scale adopted to plot the large growth of \tilde{g}_k . Finally we notice that, going from Figs. 3 to Fig. 4, no qualitative change in the flow is observed, but only more pronounced changes of the variables u_k and \tilde{g}_k .

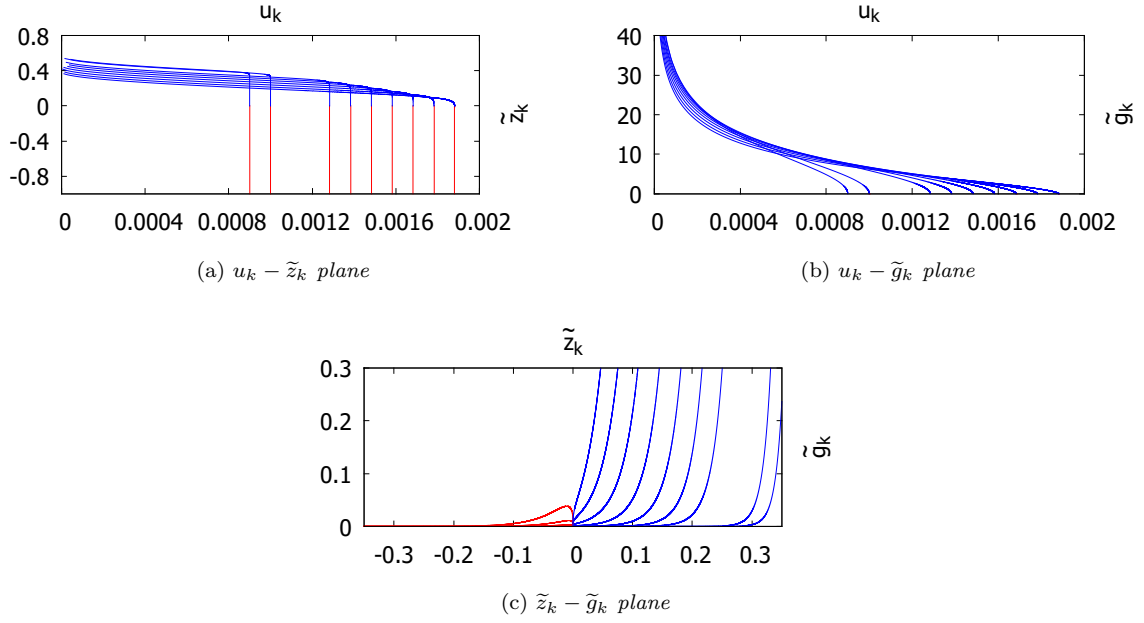


FIG. 3: Projections of the flow derived from Eqs. (19), on the three coordinate planes associated with u_k , \tilde{z}_k , \tilde{g}_k . The initial points have different values of u_k , but $\tilde{g}_k = 10^{-3}$ for all lines, while $\tilde{z}_k = -10^{-7}$ for lines that flow toward large negative \tilde{z}_k (red lines for online figures) and $\tilde{z}_k = 0$ for those that flow toward positive \tilde{z}_k (blue lines for online figures). Note that in plot (b) only the latter blue curves with positive \tilde{z}_k are visible due to the scale used on the \tilde{g}_k axis.

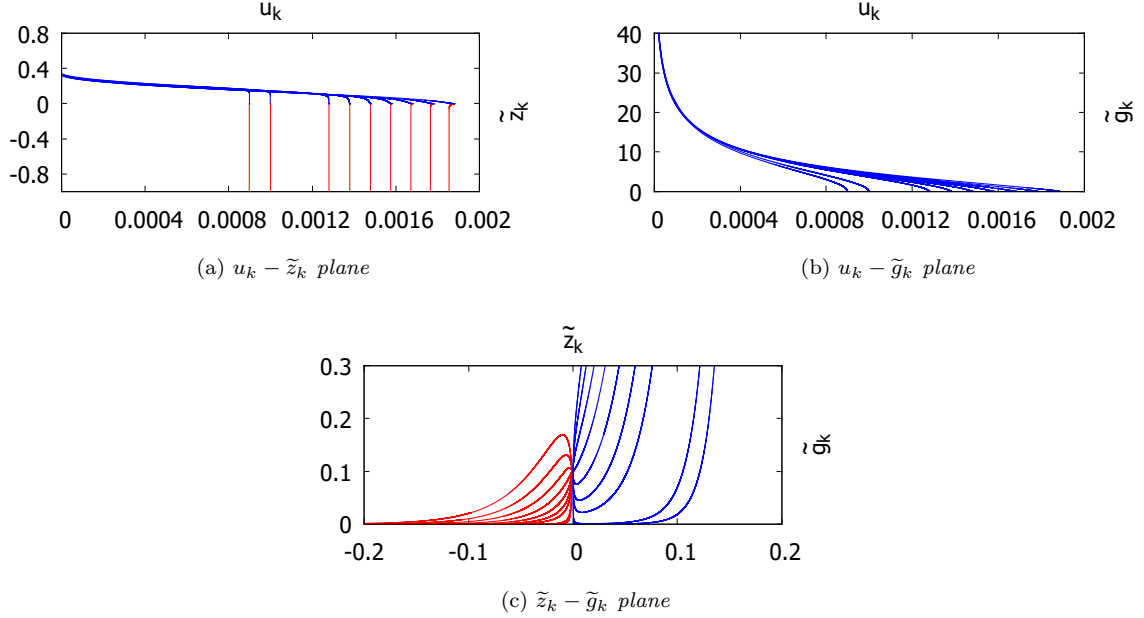


FIG. 4: Same as in Fig. 3, but $\tilde{g}_k = 10^{-1}$ in all cases, while $\tilde{z}_k = -10^{-3}$ for lines that flow toward large negative \tilde{z}_k (red curves for online figures) and $\tilde{z}_k = -10^{-4}$ for those that flow toward positive \tilde{z}_k (blue curves for online figures). As in Fig. 3, in plot (b) only the latter blue curves with positive \tilde{z}_k are visible due to the scale used on the \tilde{g}_k axis.

IV. COMPLETE FLOW EQUATIONS

Once we have a definite picture of the truncated flow in Eqs. (19) which is certainly reliable for small couplings \tilde{z}_k, \tilde{g}_k , we switch to the study of the complete RG beta-functions (15), whose explicit form is displayed in Eqs. (A11), (A16), (A19). Even if not evident from these three equations, properties observed in the truncated case in (19) for small \tilde{g}_k, \tilde{z}_k must obviously hold even in the general case in the same regime.

Therefore, the line of fixed points at $\tilde{g}_k = \tilde{z}_k = 0$ is still present in Eqs. (A11), (A16), (A19) and the properties of this line of points, already discussed for the truncated equations, remain unchanged also when the complete flow equations are considered. In addition, close to this axis, in Figs. 5 and 6 we can deduce again the presence of a separatrix manifold between the two phases characterised by positive (blue curves for online figures) or negative (red curves for online figures) \tilde{z}_k for growing $t = \log(\Lambda/k)$.

As for the truncated flow, by comparing Figs. 5 and 6, we see again a swifter evolution of the three parameters in the latter case, i.e. for larger initial value of \tilde{g}_k . So, in this regime, no qualitative difference appears with respect to Eqs. (19).

However, a clear difference is evident in the (blue) phase with positive \tilde{z}_k , when confronting Figs. 5, 6 with Figs. 3, 4. In fact in the latter case, \tilde{g}_k grows to very large values while u_k is constantly decreasing and the curves are interrupted only when they hit a spinodal point with $u_k = 0$ and, consequently, $\partial_t \tilde{g}_k = \infty$; in the complete flow instead, a weak dependence of u_k on the flow, especially for smaller values of \tilde{g}_k (see Fig. 5), and, more importantly, the curves get stopped at points that have rather small values of \tilde{g}_k and \tilde{z}_k , well before u_k could reach zero.

The interruption of the curves in the phase with positive \tilde{z}_k is possibly due to a breakdown of the numerical procedure adopted to integrate the equations because the exponential factors appearing in Eqs. (A11), (A16), (A19) become too large to be handled. As it is visible especially in plot (a) and (c) of Figs. 5, 6, this occurs approximately for $\tilde{z}_k \simeq 0.07 \div 0.1$, depending on the value of \tilde{g}_k . Actually, we did not attempt to solve or avoid this numerical problem, as in any case we observe that the flow in this regime yields increasing \tilde{g}_k and decreasing u_k and it is evident, at least from Eq. (A19), that values $\tilde{g}_k > 1$ produce complex numbers in the right-hand side of the equation, while $u_k = 0$ corresponds to a spinodal point where $\partial_t \tilde{g}_k$ diverges. Therefore, the set of flow equations (A11), (A16), (A19), in the phase with positive \tilde{z}_k is anyway plagued by singularities.

Instead, we now focus on the other phase with $\tilde{z}_k < 0$, which is much smoother and the flow trajectories are easily prolonged down to $k \rightarrow 0$ with \tilde{g}_k that gets rapidly suppressed in that limit, while u_k stays practically unchanged and $\tilde{z}_k \rightarrow -\infty$. It is interesting to check the behavior of g_k and z_k , related to \tilde{g}_k and \tilde{z}_k by Eq. (14). It is easy to verify that $g_k \rightarrow 0$, because of Eq. (14), while z_k requires an explicit computation, and we report its plot as a function of k for the three flows already examined in Figs. 5, 6, respectively in plot (a) and (c) of Fig. 7. Now it is evident that z_k is finite in the limit $k \rightarrow 0$ and it has also become constant when k approaches zero, as shown by the formation of plateaus in this limit. Actually, even the two upper curves in plot (a) have such a plateau, but it becomes visible only at smaller k as it is shown in the enlargement displayed in plot (b): the constant value is reached around $k \simeq 2 \cdot 10^{-3}$ for the lower curve and $k \simeq 10^{-3}$ for the upper curve.

These results represent a crucial starting point to consider the IR limit of the model (3) and to analyse how it is described from the point of view of the standard two-derivative four-dimensional sine-Gordon model. In fact, in the latter model the scaling dimensions of the operators are set by using the two-derivative term as the leading reference operator and this clearly produces a different scaling with respect to the one set in Eq. (14) to determine the flow, with dimensionless field φ and dimensionless $u_k = \tilde{u}_k$.

Therefore, we go back to Eq. (1) and require the field Φ to have the dimension of an energy; consequently, to maintain dimensionless the argument of the cosine, β must have the dimension of an inverse energy and, since it must be RG scale independent, we can use it to set a definite mass scale M that specifies the IR regime of the model :

$$\beta_M = \frac{1}{M} \quad (20)$$

Then accordingly, the IR average effective action is

$$\Gamma_k^{IR}[\Phi] = \int d^4x \left[\frac{w_k}{2} \Delta\Phi(x)\Delta\Phi(x) + \frac{Z_k}{2} \partial_\mu\Phi(x)\partial_\mu\Phi(x) + g_k (1 - \cos \beta_M \Phi) \right] \quad (21)$$

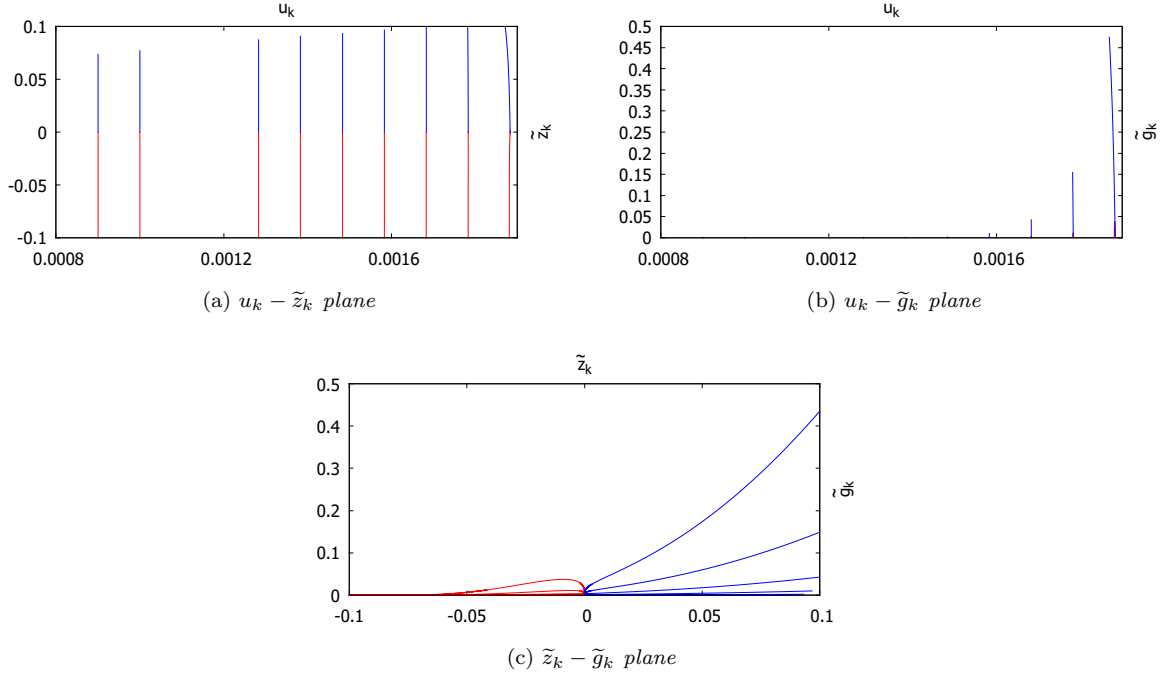


FIG. 5: Projections of the flow derived from Eqs. (A11), (A16), (A19), on the three coordinate planes associated with u_k , \tilde{z}_k , \tilde{g}_k . The initial points have $\tilde{g}_k = 10^{-3}$ for all lines, while $\tilde{z}_k = -10^{-7}$ for lines with $\tilde{z}_k < 0$ (red lines for online figures) and $\tilde{z}_k = 10^{-7}$ for those with $\tilde{z}_k > 0$ (blue lines for online figures). As in Fig. 3, only the latter blue curves with $\tilde{z}_k > 0$ are visible in plot (b).

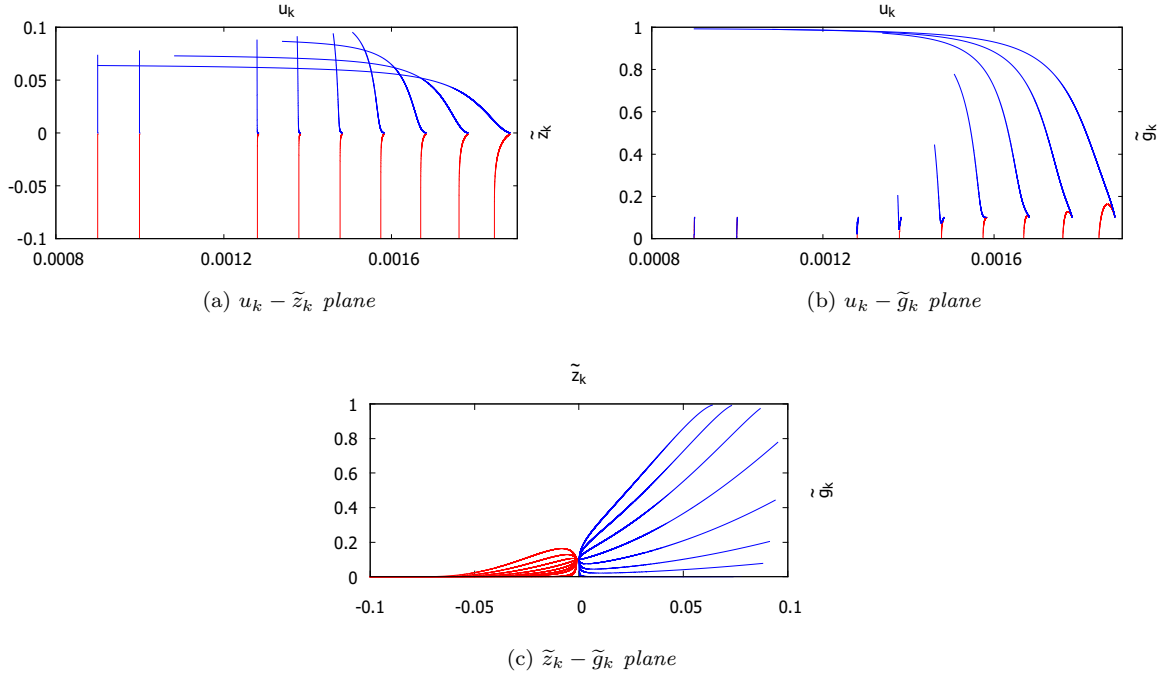


FIG. 6: Same as in Fig. 5, but with initial values $\tilde{g}_k = 10^{-1}$ for all lines while $\tilde{z}_k = -10^{-3}$ for curves with $\tilde{z}_k < 0$ (red online) and $\tilde{z}_k = 10^{-7}$ for curves with $\tilde{z}_k > 0$ (blue online).

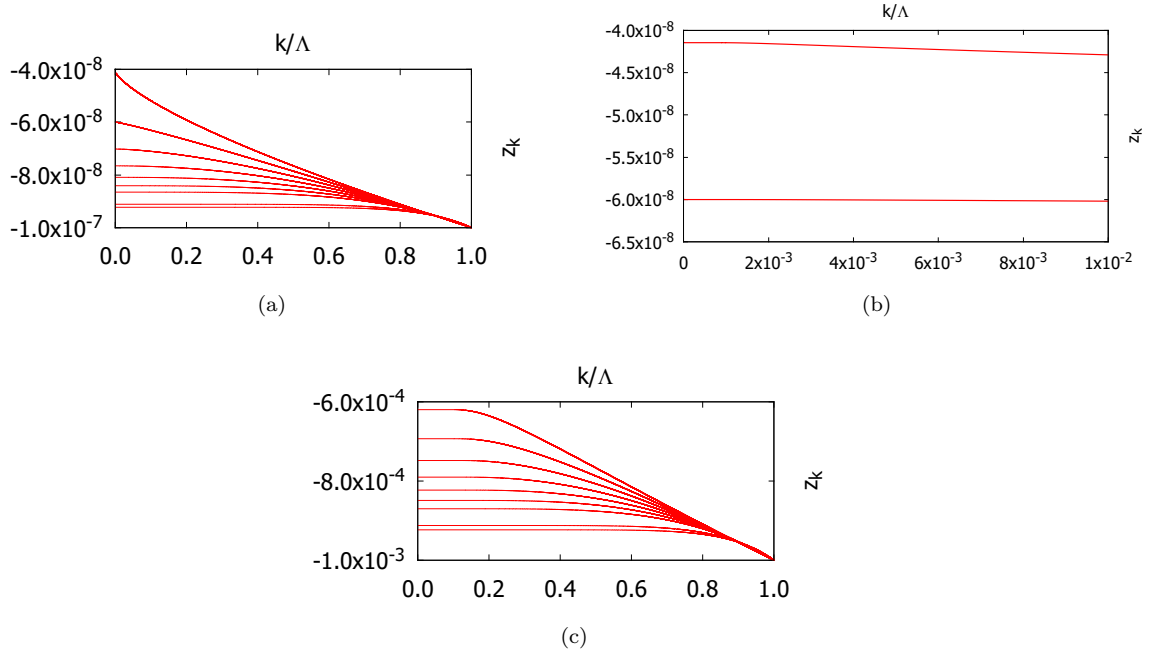


FIG. 7: Flow of $z_k = k^2 \tilde{z}_k$. Lines are plotted accordingly to the coding of the previous figures, respectively referring to the $\tilde{z}_k < 0$ (red online) phase in Fig.5 (plot (a)) and Fig.6 (plot (c)). Plot (b) shows the enlargement of a detail of plot (a).

and the dimension of the two couplings of the derivative terms in energy units are : $[Z_k] = 0$, $[w_k] = -2$, while the coupling g_k coincides with that in Eq. (3) and therefore $[g_k] = 4$, and the rescaled field defined in Eq. (2), $\varphi = \beta_M \Phi$, is dimensionless.

In order to make contact between the flow in Eq. (3) and in Eq. (21), it is sufficient to rewrite the field Φ in terms of φ in the latter, according to Eq. (2), and then equate the two expressions. Thus, we find the relations

$$\frac{w_k}{\beta_M^2} = u_k = \tilde{u}_k \quad ; \quad \frac{Z_k}{\beta_M^2} = z_k = \tilde{z}_k k^2, \quad (22)$$

which express the parameters w_k and Z_k in terms of \tilde{u}_k and \tilde{z}_k in the regime $k < M$.

From Eq. (22) and Fig.7 we conclude that Z_k is a constant in the limit $k \rightarrow 0$. Also w_k is constant in the IR limit, so that, this parameter expressed in units of the running scale k goes like $\tilde{w}_k \equiv w_k k^2 = u_k k^2/M^2$, i.e. vanishes in the limit $k \rightarrow 0$. In addition, as already observed, both g_k and \tilde{g}_k vanish in the same limit and one concludes that the IR limit of the model (3), described in terms of the effective model in Eq. (21), reduces to the two-derivative kinetic term with a finite multiplicative coefficient Z_k , which is nothing else than the Gaussian model, but with the essential difference that in this case $Z_k < 0$.

V. CONCLUDING REMARKS

We studied the generalized higher-derivative sine-Gordon model in Eq. (1), which includes a four-derivative plus a two-derivative kinetic term, in 4D and we obtained an improved picture of its phase diagram, with respect to the model discussed in [58] where the two-derivative term is omitted. In [58], it was observed that, despite the similarities with the 2D BKT transition and despite the possibility of constructing topological configurations analogous to the 2D vortices, the phase diagram obtained in that case shows a significant difference with respect to the BKT one. In fact, although a line of fixed points is found, including a critical point at $u_k = u_k^*$ that separates a subset of attractive from another subset of repulsive fixed points, yet the negative sign appearing in the right hand side of one of the flow equations

does make all flow trajectories homogeneous (as shown in Fig 1), without a distinction of two separate phases, as occurs instead in the 2D BKT diagram.

When the full model, Eq. (1), is taken into account, it becomes clear that the two-derivative operator proportional to z_k , a relevant coupling, is essential in determining the separation of two phases, which are realised in the IR limit for different signs of \tilde{z}_k , and the line characterised by $\tilde{z}_k = \tilde{g}_k = 0$ and $u_k > u_k^*$ is a set of UV attractive fixed points with all trajectories departing from it when the RG scale is lowered.

In the adopted scheme, the phase displaying $\tilde{z}_k > 0$ shows some pathologies, such as the presence of spinodal points or regions where RG equations become non-analytic, that make the IR limit $k \rightarrow 0$ impossible to achieve, and this suggests that the model in Eq. (3) could be insufficient to properly describe the $\tilde{z}_k > 0$ phase. Conversely, the opposite case with $\tilde{z}_k < 0$ is totally under control and the RG flow generated by the action in Eq. (3) is regular in the IR limit and, with the help of a mapping on an effective model, built around the Gaussian fixed point, we verified that our system reduces to a Gaussian model in this limit, but with negative $\tilde{z}_k < 0$.

The use of another effective model to analyse the IR limit, is in fact inspired by the work in [66] where this approach is used to discuss the flow from an UV to an IR “Gaussian fixed point”, both associated to a scalar model containing, in addition to the two-derivative term $z_1(\partial\phi\partial\phi)$, a pair of four-derivative terms, namely $z_2(\partial^2\phi\partial^2\phi)$ and $z_3(\partial\phi\partial\phi)^2$, with the inessential difference that in [66], instead of directly looking at the flow of z_1 and z_2 (as in our analysis), the flow of the anomalous dimensions associated to these couplings is studied. Incidentally, we remark that, in our analysis, we could also have included the term proportional to z_3 , to account for an even more general model, but, because of the result shown in [66] on the beta-function of the dimensionless coupling $\tilde{z}_3 : \beta_{\tilde{z}_3} \propto \tilde{z}_3$, i.e. $\tilde{z}_3 = 0$ is a stationary point for this variable, we preferred to maintain z_3 turned off and focus on model (1), which already contains a definite phase structure.

In [66], trajectories connecting the UV Gaussian point (whose appearance is due to the presence of the higher derivative terms) to the IR Gaussian point (related to the presence of the two-derivative term) are in fact pointed out and this is in contrast with our findings, where a consistent IR limit requires $\tilde{z}_k < 0$. However, this should not come as a surprise, because our result strictly depends on the presence of the sine-Gordon potential and on the flow of the coupling \tilde{g}_k , which is instead absent in the former analysis.

Actually, the resulting negative value $\tilde{z}_k < 0$ in the IR makes the higher derivative model (1) interesting. In fact, the contrast of a positive higher-derivative and a negative two-derivative term, can generate a non-uniform modulated ground state and the associated excitations have to be constructed upon this peculiar background.

Then, it is noticeable that such a model has a few points in common with scalar models of conformally reduced Euclidean gravity, where an UV fixed point is found [67–70], ensuring the non-perturbative renormalizability of the theory, while the sign in front of the two-derivative term turns out to be negative, as it occurs in our analysis. It has also been suggested that higher derivative terms could cure the instability produced by the negative kinetic term [71]. In addition, even some evidence that a continuous line of UV fixed points could be present for such a model, when analysed within an improved approximation scheme [72, 73]. Despite the structural differences of the two issues, concerning in particular the form of the potential, all these mentioned features clearly resemble the findings here discussed for the higher derivative sine-Gordon model and, therefore, further investigation about this point is certainly worthwhile.

ACKNOWLEDGEMENTS

GGNA acknowledges support from the project PRIN 2022 - 2022XK5CPX (PE3) SoS-QuBa - “Solid State Quantum Batteries: Characterization and Optimization”. DZ gratefully acknowledges A. Bonanno for enlightening discussions.

Appendix A: Determination of the RG flow equations

We start with some useful formulae. Given the four-momenta p_μ, q_μ appearing in the various n-point functions, let us define θ the angle between p_μ and q_μ , $p \equiv \sqrt{p^2}$, $q \equiv \sqrt{q^2}$, $y = (p + q)^2$ and, by means of the derivation of a composite function we get

$$\frac{d^2}{dp^2} = \left(\frac{dy}{dp}\right)^2 \frac{d^2}{dy^2} + \frac{d^2 y}{dp^2} \frac{d}{dy} \quad (\text{A1})$$

$$\frac{d^4}{dp^4} = \left(\frac{dy}{dp}\right)^4 \frac{d^4}{dy^4} + 6 \left(\frac{dy}{dp}\right)^2 \frac{d^2 y}{dp^2} \frac{d^3}{dy^3} + 3 \left(\frac{d^2 y}{dp^2}\right)^2 \frac{d^2}{dy^2} \quad (\text{A2})$$

and, when the derivatives are computed at $p = 0$, we find $y'(p)|_{p=0} = 2q \cos(\theta)$ and $y''(p)|_{p=0} = 2$. For $G_k(y) = (u_k y^2 + z_k y + V_k'' + k^4)^{-1}$:

$$\begin{aligned} \frac{\partial G_k(y)}{\partial y} &= -(2u_k y + z_k) G_k(y)^2 \\ \frac{\partial^2 G_k(y)}{\partial y^2} &= 2(2u_k y + z_k)^2 G_k(y)^3 - 2u_k G_k(y)^2 \\ \frac{\partial^3 G_k(y)}{\partial y^3} &= 12u_k (2u_k y + z_k) G_k(y)^3 - 6(2u_k y + z_k)^3 G_k(y)^4 \\ \frac{\partial^4 G_k(y)}{\partial y^4} &= 24u_k^2 G_k(y)^3 + 24(2u_k y + z_k)^4 G_k(y)^5 - 72u_k (2u_k y + z_k)^2 G_k(y)^4. \end{aligned} \quad (\text{A3})$$

Finally, in order to avoid the extremely lengthy integration of hypergeometric functions we resort to the Schwinger representation:

$$\frac{1}{A^n} = \int_0^\infty ds \frac{s^{n-1}}{(n-1)!} \exp(-sA). \quad (\text{A4})$$

and we shall also use the following results to integrate out the field φ :

$$-\frac{1}{2\pi} \int_{-\pi}^{\pi} d\varphi \cos \varphi e^{-s\tilde{g}_k \cos \varphi} = I_1(\tilde{g}_k s), \quad (\text{A5a})$$

$$\frac{1}{2\pi} \int_0^{2\pi} d\varphi \sin^2 \varphi e^{-s\tilde{g}_k \cos \varphi} = \frac{I_1(\tilde{g}_k s)}{\tilde{g}_k s}, \quad (\text{A5b})$$

$$\frac{1}{2\pi} \int_0^{2\pi} d\varphi \sin^2 \varphi \cos \varphi e^{-s\tilde{g}_k \cos \varphi} = -\frac{I_2(\tilde{g}_k s)}{\tilde{g}_k s}, \quad (\text{A5c})$$

$$\frac{1}{2\pi} \int_0^{2\pi} d\varphi \sin^2 \varphi \cos^2 \varphi e^{-s\tilde{g}_k \cos \varphi} = \frac{\tilde{g}_k s I_1(\tilde{g}_k s) - 3I_2(\tilde{g}_k s)}{\tilde{g}_k^2 s^2}. \quad (\text{A5d})$$

where $I_a(x)$ is the modified Bessel function of the first kind [74].

1. The equation for \tilde{u}_k

The flow equation for $\tilde{u}_k = u_k$, is obtained from (12) (note that the integral is written in d dimensions and only at the end of the computation we shall specialise it to $d = 4$) and from (A2) and its structure is $P_0[U_1 + U_2 + U_3]$ where P_0 is given in Eq. (11) and the three terms U_1, U_2, U_3 are respectively related to the second, the third, and the fourth derivative of $G_k(y)$ with respect to y .

After carrying out the field integration by making use of (A5b) and (A5c), we obtain for $P_0 U_1$ (here

$y = q^2$):

$$\begin{aligned} & \frac{P_0}{2} \int \frac{d^d q}{(2\pi)^d} \partial_t R_k g_k^2 \sin^2 \varphi \left[2(2u_k q^2 + z_k)^2 G_k^5(q^2) - 2u_k G_k^4(q^2) \right] = \\ & - \frac{4dk^{d-4}\tilde{g}_k^2}{(4\pi)^{d/2}\Gamma(1+d/2)} \int_0^{2\pi} d\varphi \int_0^\infty dq q^{d-1} \sin^2 \varphi \frac{3u_k^2 q^4 + 3u_k \tilde{z}_k q^2 + \tilde{z}_k^2 - u_k - u_k \tilde{g}_k \cos \varphi}{(u_k q^4 + \tilde{z}_k q^2 + \tilde{g}_k \cos \varphi + 1)^5} = \\ & - \int_0^\infty ds \int_0^\infty dy y^{d/2-1} \frac{s^4 k^{d-4} d\tilde{g}_k^2 e^{-s(1+u_k y^2 + \tilde{z}_k y)}}{12(4\pi)^{d/2}\Gamma(1+d/2)} \left[\frac{(3u_k^2 y^2 + 3u_k \tilde{z}_k y + \tilde{z}_k^2 - u_k) I_1(\tilde{g}_k s)}{\tilde{g}_k s} + \frac{u_k I_2(\tilde{g}_k s)}{s} \right]. \end{aligned} \quad (\text{A6})$$

Then momentum integration cannot be performed for generic dimension d but, by taking the limit $d \rightarrow 4^+$ before performing the proper time integral we find (Erf (z) is the error function [74])

$$\begin{aligned} P_0 U_1 = & \int_0^\infty ds \frac{\tilde{g}_k e^{-s} s}{1536\pi^2 u_k^2} \left\{ I_1(\tilde{g}_k s) \left[\sqrt{\pi} \sqrt{s u_k} \tilde{z}_k e^{\frac{s \tilde{z}_k^2}{4u_k}} \left((4s-6)u_k - s \tilde{z}_k^2 \text{Erf} \left(\frac{\sqrt{s} \tilde{z}_k}{2\sqrt{u_k}} \right) + \right. \right. \right. \\ & \left. \left. \left. 8(s-3)u_k^2 - 2u_k \tilde{z}_k \left(\sqrt{\pi} (2s-3) \sqrt{s u_k} e^{\frac{s \tilde{z}_k^2}{4u_k}} + s \tilde{z}_k \right) + \sqrt{\pi} s \tilde{z}_k^3 \sqrt{s u_k} e^{\frac{s \tilde{z}_k^2}{4u_k}} \right) \right] - \right. \\ & \left. 4\tilde{g}_k s u_k I_2(\tilde{g}_k s) \left(\sqrt{\pi} \sqrt{s u_k} \tilde{z}_k e^{\frac{s \tilde{z}_k^2}{4u_k}} \text{Erf} \left(\frac{\sqrt{s} \tilde{z}_k}{2\sqrt{u_k}} \right) - \sqrt{\pi} \tilde{z}_k \sqrt{s u_k} e^{\frac{s \tilde{z}_k^2}{4u_k}} + 2u_k \right) \right\}. \end{aligned}$$

Analogously, for $P_0 U_2$ we find

$$\begin{aligned} & \frac{P_0}{4!} \int \frac{d^d q}{(2\pi)^d} \partial_t R_k g_k^2 \sin^2 \varphi \cos^2 \theta 48q^2 \left(12u_k(2u_k q^2 + z_k) G_k^5(q^2) - 6(2u_k q^2 + z_k)^3 G_k^6(q^2) \right) = \\ & - \frac{8k^{d-4}\tilde{g}_k^2}{(4\pi)^{d/2}\Gamma(1+d/2)} P_0 \int_0^\infty dq q^{d+1} \sin^2 \varphi \left[(12u_k(2u_k q^2 + \tilde{z}_k)(u_k q^4 + \tilde{z}_k q^2 + 1) - 6(2u_k q^2 + \tilde{z}_k)^3) \right. \\ & \left. + 12u_k \tilde{g}_k (2u_k q^2 + \tilde{z}_k) \cos \varphi \right] G_k^6(q^2), \end{aligned} \quad (\text{A7})$$

Then, by performing the field integration through (A5b) and (A5c), the momenta integration and by taking the limit $d \rightarrow 4^+$ we get:

$$\begin{aligned} P_0 U_2 = & \int_0^\infty ds \frac{\tilde{g}_k e^{-s} s}{640\pi^2 u_k^{3/2}} \left(\sqrt{\pi} \sqrt{s} \tilde{z}_k e^{\frac{s \tilde{z}_k^2}{4u_k}} \left(\text{Erf} \left(\frac{1}{2} \tilde{z}_k \sqrt{\frac{s}{u_k}} \right) - 1 \right) \times \right. \\ & \left(I_1(\tilde{g}_k s) \left((6-4s)u_k + s \tilde{z}_k^2 \right) + 4\tilde{g}_k s u_k I_2(\tilde{g}_k s) \right) + \\ & \left. 2\sqrt{u_k} \left(I_1(\tilde{g}_k s) \left(s \tilde{z}_k^2 - 4(s-2)u_k \right) + 4\tilde{g}_k s u_k I_2(\tilde{g}_k s) \right) \right). \end{aligned} \quad (\text{A8})$$

For the term $P_0 U_3$ we have

$$\begin{aligned} & \frac{P_0}{4!} \int \frac{d^d q}{(2\pi)^d} \partial_t R_k g_k^2 \sin^2 \varphi \cos^4 \theta 16q^4 \times \\ & \left(24(2u_k q^2 + z_k)^4 G_k^7(q^2) - 72u_k(2u_k q^2 + z_k)^2 G_k^6(q^2) + 24u_k^2 G_k^5(q^2) \right) = \\ & - \frac{64k^{d-4}3\tilde{g}_k^2}{4!(d+2)(4\pi)^{d/2}\Gamma(1+d/2)} P_0 \int_0^\infty dq q^{d+3} \left[24(2u_k q^2 + \tilde{z}_k)^4 - \right. \\ & \left. 72u_k(2u_k q^2 + \tilde{z}_k)^2(u_k q^4 + \tilde{z}_k q^2 + \tilde{g}_k \cos \varphi + 1) + 24u_k^2(u_k q^4 + \tilde{z}_k q^2 + \tilde{g}_k \cos \varphi + 1)^2 \right] G_k^7(q^2). \end{aligned} \quad (\text{A9})$$

The integration over φ is done with the help of (A5b), (A5c) and also (A5d). Finally, by integrating over the momenta e performing the limit $d \rightarrow 4^+$ we obtain the third contribution to the flow of u_k (Erfc (z) is the complementary error function [74]):

$$\begin{aligned}
P_0 U_3 = & \int_0^\infty ds \frac{g e^{-s}}{368640 \pi^2 u_k^4} \left\{ I_1(\tilde{g}_k s) \left[\sqrt{\pi} \tilde{z}_k e^{\frac{s \tilde{z}_k^2}{4 u_k}} \text{Erfc} \left(\frac{1}{2} \tilde{z}_k \sqrt{\frac{s}{u_k}} \right) \left(8 s^2 \tilde{z}_k^2 (s u_k)^{3/2} (2(\tilde{g}_k^2 + 1) u_k - \tilde{z}_k^2) + \right. \right. \right. \\
& 2 s (s u_k)^{3/2} \left(48(\tilde{g}_k^2 + 1) u_k^2 - 64 u_k \tilde{z}_k^2 + 13 \tilde{z}_k^4 \right) + \tilde{z}_k^6 \sqrt{s^7 u_k} + 1800 \sqrt{s u_k^7} + \\
& \left. \left. 60 u_k (s u_k)^{3/2} (7 \tilde{z}_k^2 - 24 u_k) \right) + 2 u_k \left(-64 u_k^3 (s(\tilde{g}_k^2 s + s - 20) + 30) - \right. \right. \\
& \left. \left. 4 s u_k^2 \tilde{z}_k^2 (4 s(\tilde{g}_k^2 s + s - 7) + 95) - s^3 \tilde{z}_k^6 + 8(s - 3) s^2 u_k \tilde{z}_k^4 \right) \right] + \\
& 8 \tilde{g}_k s u_k^{3/2} I_2(\tilde{g}_k s) \left[\sqrt{\pi} \sqrt{s} \tilde{z}_k e^{\frac{s \tilde{z}_k^2}{4 u_k}} \left(s^2 \tilde{z}_k^4 - 24(s - 6) u_k^2 + 2 s(5 - 2 s) u_k \tilde{z}_k^2 \right) \text{Erfc} \left(\frac{1}{2} \tilde{z}_k \sqrt{\frac{s}{u_k}} \right) + \right. \\
& \left. \left. 2 \sqrt{u_k} \left(-s^2 \tilde{z}_k^4 + 8(2 s - 17) u_k^2 + 4(s - 2) s u_k \tilde{z}_k^2 \right) \right] \right\}. \tag{A10}
\end{aligned}$$

The sum of the three contributions yields the flow equation for u_k :

$$\partial_t u_k = \int_0^\infty ds \frac{\tilde{g} s e^{-s}}{368640 \pi^2 u_k^4} [c_1 I_1(\tilde{g}_k s) + c_2 I_2(\tilde{g}_k s)], \tag{A11}$$

where

$$\begin{aligned}
c_1 = & \left(\sqrt{\pi} \tilde{z}_k e^{\frac{s \tilde{z}_k^2}{4 u_k}} \text{Erfc} \left(\frac{1}{2} \tilde{z}_k \sqrt{\frac{s}{u_k}} \right) \left(8 s^2 \tilde{z}_k^2 (s u_k)^{3/2} (2(\tilde{g}_k^2 + 1) u_k - \tilde{z}_k^2) \right. \right. \\
& + 2 s (s u_k)^{3/2} \left(48(\tilde{g}_k^2 + 1) u_k^2 - 64 u_k \tilde{z}_k^2 + 13 \tilde{z}_k^4 \right) + \tilde{z}_k^6 \sqrt{s^7 u_k} - 216 \sqrt{s u_k^7} \\
& + 12 u_k (s u_k)^{3/2} (7 \tilde{z}_k^2 - 8 u_k) \left. \right) + 2 u_k \left(-64 u_k^3 ((\tilde{g}_k^2 + 1) s^2 + s + 3) \right. \\
& \left. \left. - 4 s u_k^2 \tilde{z}_k^2 (4 s(\tilde{g}_k^2 s + s - 7) + 11) - s^3 \tilde{z}_k^6 + 8(s - 3) s^2 u_k \tilde{z}_k^4 \right) \right); \\
c_2 = & 8 \tilde{g}_k s u_k^{3/2} \left(\sqrt{\pi} \sqrt{s} \tilde{z}_k e^{\frac{s \tilde{z}_k^2}{4 u_k}} \left(s^2 \tilde{z}_k^4 - 24(s + 1) u_k^2 + 2 s(5 - 2 s) u_k \tilde{z}_k^2 \right) \right. \\
& \left. \left. \text{Erfc} \left(\frac{1}{2} \tilde{z}_k \sqrt{\frac{s}{u_k}} \right) + 2 \sqrt{u_k} \left(-s^2 \tilde{z}_k^4 + 16(s + 2) u_k^2 + 4(s - 2) s u_k \tilde{z}_k^2 \right) \right) \right).
\end{aligned}$$

2. The equation for \tilde{z}_k

To calculate the flow equation of \tilde{z}_k we start from Eq. (13) (note that the integral is written in d dimensions and only at the end of the computation we shall specialise it to $d = 4$) and , from Eq. (A1), we notice that its structure in this case is of the form: $P_0[Z_1 + Z_2]$, where, as before, Z_1 is related to the first derivative, while Z_2 is related to the second derivative of $G_k(y)$. By proceeding as for the u_k case,

we get

$$\begin{aligned}
& \frac{P_0}{2!} \int \frac{d^d q}{(2\pi)^d} \partial_t R_k g_k^2 \sin^2 \varphi \left(- (2u_k q^2 + z_k) G_k^4(q^2) \right) = \\
& \frac{k^{d-2} \tilde{g}_k^2 4d}{(4\pi)^{d/2} \Gamma(1+d/2)} \int_0^\infty ds \frac{s^3}{3!} P_0 \int_0^\infty dq q^{d-1} \sin^2 \varphi (2u_k q^2 + \tilde{z}_k) e^{-s(u_k q^4 + \tilde{z}_k q^2 + \tilde{g}_k \cos \varphi + 1)} = \\
& \frac{k^{d-2} \tilde{g}_k^2 2d}{(4\pi)^{d/2} \Gamma(1+d/2)} \int_0^\infty ds e^{-s} \frac{s^3}{3!} \int_0^\infty dy y^{d/2-1} (2u_k y + \tilde{z}_k) e^{-s(u_k y^2 + \tilde{z}_k y)} \frac{I_1(\tilde{g}_k s)}{\tilde{g}_k s}, \quad (\text{A12})
\end{aligned}$$

where in the last term we performed the field integration via Eq. (A5b) and, again, $y = q^2$. After performing the momentum integration and taking the limit $d \rightarrow 4^+$, we find :

$$P_0 Z_1 = \int_0^\infty ds \left[- \frac{\tilde{g}_k k^2 s I_1(\tilde{g}_k s) e^{\frac{1}{4}s \left(\frac{\tilde{z}_k^2}{u_k} - 4 \right)} \left(\text{Erf} \left(\frac{1}{2} \tilde{z}_k \sqrt{\frac{s}{u_k}} \right) - 1 \right)}{48\pi^{3/2} \sqrt{s u_k}} \right]. \quad (\text{A13})$$

We now turn to $P_0 Z_2$ and, after integrating the angular part and making use of Eqs. (A5b), (A5c), (A5d), to integrate the field φ , we obtain

$$\begin{aligned}
& \frac{P_0}{2!} \int \frac{d^d q}{(2\pi)^d} \partial_t R_k g_k^2 \sin^2 \varphi 4q^2 \cos^2 \theta (2(2u_k q^2 + z_k)^2 G^5(q) - 2u_k G^4(q)) = \\
& - \frac{8k^{d-2} \tilde{g}_k^2}{(4\pi)^{d/2} \Gamma(1+d/2)} \int_0^\infty ds e^{-s} \frac{s^4}{4!} P_0 \int_0^\infty q^{d+1} e^{-s(u_k q^4 + \tilde{z}_k q^2 + \tilde{g}_k \cos \varphi)} \times \\
& 2 \sin^2 \varphi (3u_k^2 q^4 + 3u_k \tilde{z}_k q^2 + \tilde{z}_k^2 - u_k - u_k \tilde{g}_k \cos \varphi) = \\
& - \frac{8k^{d-2} \tilde{g}_k^2}{(4\pi)^{d/2} \Gamma(1+d/2)} \int_0^\infty ds e^{-s} \frac{s^4}{4!} \int_0^\infty dy y^{d/2} e^{-s(u_k y^2 + \tilde{z}_k y)} \times \\
& \left((3u_k^2 y^2 + 3u_k \tilde{z}_k y + \tilde{z}_k^2 - u_k) \frac{I_1(\tilde{g}_k s)}{\tilde{g}_k s} + u_k \frac{I_2(\tilde{g}_k s)}{s} \right). \quad (\text{A14})
\end{aligned}$$

Performing the momentum integration and taking the limit $d \rightarrow 4^+$ yield

$$\begin{aligned}
P_0 Z_2 = & - \int_0^\infty ds \frac{\tilde{g}_k k^2 \sqrt{s} e^{-s}}{3072\pi^2 u_k^{5/2} \tilde{z}_k} \left\{ I_1(\tilde{g}_k s) \left[\tilde{z}_k \left(-2\tilde{z}_k^3 \sqrt{s^3 u_k} + \sqrt{\pi} e^{\frac{s \tilde{z}_k^2}{4u_k}} \left[s^2 \tilde{z}_k^4 \right. \right. \right. \right. \\
& + 4(9-2s)u_k^2 - 4(s-2)su_k \tilde{z}_k^2 \left. \left. \left. \right] - 12\tilde{z}_k \sqrt{s u_k^3} + 8\tilde{z}_k (s u_k)^{3/2} \right) \right. \\
& \left. \left. - \sqrt{\pi} \tilde{z}_k e^{\frac{s \tilde{z}_k^2}{4u_k}} \left(s^2 \tilde{z}_k^4 + 4(9-2s)u_k^2 - 4(s-2)su_k \tilde{z}_k^2 \right) \text{Erf} \left(\frac{1}{2} \sqrt{\frac{s \tilde{z}_k^2}{u_k}} \right) \right] \right\} \\
& + 4\tilde{g}_k s u_k \sqrt{\tilde{z}_k^2} I_2(\tilde{g}_k s) \left[\sqrt{\pi} e^{\frac{s \tilde{z}_k^2}{4u_k}} (s \tilde{z}_k^2 + 2u_k) \text{Erfc} \left(\frac{1}{2} \tilde{z}_k \sqrt{\frac{s}{u_k}} \right) - 2\tilde{z}_k \sqrt{s u_k} \right]. \quad (\text{A15})
\end{aligned}$$

Finally, the sum of Eq. (A13) and Eq. (A15) provide the flow equation for \tilde{z}_k

$$\partial_t \tilde{z}_k = 2\tilde{z}_k + \int_0^\infty ds \frac{\tilde{g}_k e^{-s} (c_3 I_1(\tilde{g}_k s) - c_4 I_2(\tilde{g}_k s))}{3072\pi^2}, \quad (\text{A16})$$

where we used:

$$\begin{aligned}
c_3 &= \frac{\sqrt{s}}{u_k^{5/2}} \left[\sqrt{\pi} e^{\frac{s \tilde{z}_k^2}{4u_k}} \left(-s^2 \tilde{z}_k^4 + 4(2s+7)u_k^2 + 4(s-2)su_k \tilde{z}_k^2 \right) \text{Erfc} \left(\frac{1}{2} \tilde{z}_k \sqrt{\frac{s}{u_k}} \right) \right. \\
&\quad \left. + 2\tilde{z}_k \left(\tilde{z}_k^2 \sqrt{s^3 u_k} + 6\sqrt{s u_k^3} - 4(su_k)^{3/2} \right) \right]; \\
c_4 &= 4\tilde{g}_k \left(\frac{s}{u_k} \right)^{3/2} \left[\sqrt{\pi} e^{\frac{s \tilde{z}_k^2}{4u_k}} (s \tilde{z}_k^2 + 2u_k) \text{Erfc} \left(\frac{1}{2} \tilde{z}_k \sqrt{\frac{s}{u_k}} \right) - 2\tilde{z}_k \sqrt{s u_k} \right].
\end{aligned}$$

3. The equation for \tilde{g}_k

To calculate the flow equation of \tilde{g}_k we start from Eq. (6) (note that the integral is written in d dimensions and only at the end of the computation we shall specialise it to $d = 4$) and use the projector P_1 defined in Eq. (8).

$$\begin{aligned}
P_1 \partial_t V_k &= \frac{P_1}{2} \int \frac{d^d q}{(2\pi)^d} \frac{\partial_t R_k}{u_k q^4 + z_k q^2 + g_k \cos \varphi + k^4} = \\
&= -\frac{k^d 2d}{(4\pi)^{d/2} \Gamma(1+d/2)} \int_0^\infty ds e^{-s} \int_0^\infty dq q^{d-1} e^{-s(u_k q^4 + \tilde{z}_k q^2)} \left(-\frac{1}{\pi} \int_{-\pi}^\pi d\varphi \cos \varphi e^{-s \tilde{g}_k \cos \varphi} \right). \quad (\text{A17})
\end{aligned}$$

We now use Eq. (A5a) to integrate over the field, thus obtaining the following equation in terms of the variables $u_k, \tilde{z}_k, \tilde{g}_k$:

$$\partial_t \tilde{g}_k = 4\tilde{g}_k - \frac{2dk^{d-4}}{(4\pi)^{d/2} \Gamma(1+d/2)} \int_0^\infty ds \exp(-s) I_1(\tilde{g}_k s) \int_0^\infty dq^2 (q^2)^{d/2-1} \exp(-s(u_k q^4 + \tilde{z}_k q^2)). \quad (\text{A18})$$

After performing the momentum integral and taking the limit $d \rightarrow 4^+$ we find

$$\partial_t \tilde{g}_k = 4\tilde{g}_k - \frac{1 - \sqrt{1 - \tilde{g}_k^2}}{8\pi^2 u_k \tilde{g}_k} + \frac{\tilde{z}_k}{(4\pi)^2} \int_0^\infty ds e^{-s} \frac{I_1(\tilde{g}_k s)}{s u_k} \left[\sqrt{\pi} \sqrt{\frac{s}{u_k}} e^{\frac{s \tilde{z}_k^2}{4u_k}} \text{Erfc} \left(\frac{\sqrt{s \tilde{z}_k}}{2\sqrt{u_k}} \right) \right]. \quad (\text{A19})$$

Appendix B: RG flow from perturbative expansion

1. The four-dimensional case

In this Appendix we make use of the mapping, discussed in [58], between the model in Eq. (1) with $z = 0$ and a generalisation of the Coulomb gas in four dimensions, with the aim of deriving in an alternative way the RG equations for the couplings and, in particular, to show that the negative sign in Eq. (16) is actually the opposite of the sign in the two-dimensional case, as it is strictly related to the number of spatial dimensions of the problem. We start from the Hamiltonian density

$$H = \frac{\mathcal{K}}{2} \int d^4 \mathbf{r} \left[\Delta \theta(\mathbf{r}) \Delta \theta(\mathbf{r}) + \mathcal{T} \nabla_i \theta(\mathbf{r}) \nabla_i \theta(\mathbf{r}) \right] \quad (\text{B1})$$

that, in addition to the Laplacian of the field θ squared, contains an additional lower derivative term, proportional to the new coupling \mathcal{T} which will be used as a counterterm of higher order corrections appearing in our computation. As explained in Appendix B of [58] the Green's function of the square Laplacian Δ^2 in $d = 4$ is

$$\mathcal{G}(\mathbf{r} - \mathbf{r}') = \int \frac{d^4 \mathbf{r}''}{(2\pi)^2} \frac{1}{(\mathbf{r} - \mathbf{r}'')^2} \frac{1}{(\mathbf{r}'' - \mathbf{r}')^2} = -\frac{1}{2} \ln \frac{|\mathbf{r} - \mathbf{r}'|}{R} \quad (\text{B2})$$

that corresponds to the response at the point \mathbf{r} of a charge located in \mathbf{r}' while R indicates the size of the system. The right-hand side of (B2) comes from the explicit resolution of the integral.

The form of $\mathcal{G}(\mathbf{r} - \mathbf{r}')$ in Eq. (B2) comes from the general property of the Laplacian in $d = 4$ [75]

$$\Delta (\mathbf{r} - \mathbf{r}')^{-2} = - (2\pi)^2 \delta^4(\mathbf{r} - \mathbf{r}') \quad (\text{B3})$$

which gives

$$\Delta^2 \mathcal{G}(\mathbf{r} - \mathbf{r}') = (2\pi)^2 \delta^4(\mathbf{r} - \mathbf{r}') , \quad (\text{B4})$$

or equivalently

$$\Delta \ln |\mathbf{r} - \mathbf{r}'| = 2 (\mathbf{r} - \mathbf{r}')^{-2} , \quad (\text{B5})$$

$$\Delta^2 \ln |\mathbf{r} - \mathbf{r}'| = -8 \pi^2 \delta^4(\mathbf{r} - \mathbf{r}') . \quad (\text{B6})$$

Then from Eqs. (B1, B2, B4) one easily finds the following structure of the interaction hamiltonian density associated to a charge-anticharge pair, respectively located in \mathbf{r} and \mathbf{r}' :

$$H^{(2)} = H_{core} + \frac{\mathcal{K}}{2} (2\pi)^2 \ln |\mathbf{r} - \mathbf{r}'| + \frac{\mathcal{K} \mathcal{T}}{2} \int d^4 \mathbf{r}'' \frac{\ln |\mathbf{r}'' - \mathbf{r}'|}{(\mathbf{r} - \mathbf{r}'')^2} , \quad (\text{B7})$$

where H_{core} includes all self-interaction effects of each charge of the pair, which typically have the same form of the two terms $O(\mathcal{K})$ and $O(\mathcal{K}\mathcal{T})$ in Eq. (B7) when the limit $\mathbf{r} \rightarrow \mathbf{r}'$ is taken with a suitable short distance regulator.

In our computation of higher order corrections, we will not include the effects of $O(\mathcal{K}\mathcal{T})$ term of Eq. (B7) but nevertheless we retain it at the lowest order and treat it as a counterterm to cancel other terms generated in the procedure. In perturbation theory, this is justified if we assume \mathcal{K} and \mathcal{T} as small couplings of the same order, so that the $O(\mathcal{K}\mathcal{T})$ term is naturally higher order.

Then, in perturbation theory, we compute the charge-anticharge effective interaction, that includes dressing effects of their interaction with further charge-anticharge pairs. In this way, the system is kept globally neutral. Our procedure follows the demonstration developed in [63] for the BKT transition in $d = 2$, by rearranging it to our specific problem in $d = 4$ and, in particular we write down the partition function associated to the a system of interacting charge-anticharge pairs:

$$\mathcal{Z}_V = \sum_{N=0}^{\infty} \frac{y_0^{2N}}{(N!)^2} \prod_{i'=1}^{2N} \int d^4 x_{i'} e^{-H_I^{(2)}} , \quad (\text{B8})$$

where the sum is taken over N charge-anticharge pairs, and the interaction Hamiltonian $H_I^{(2)}$ of a pair is read from Eq. (B7):

$$H_I^{(2)}(|\mathbf{r} - \mathbf{r}'|) = H^{(2)} - H_{core} , \quad (\text{B9})$$

whereas the effects of H_{core} are collected in the fugacity $y_0 = e^{-H_{core}}$, associated to the single charge self-energy. All lengths expressed in units of the lattice spacing a .

The effective interaction $H_{eff}^{(2)}$ of a charge-anticharge pair, located at \mathbf{r} and \mathbf{r}' is given by

$$e^{-H_{eff}^{(2)}(|\mathbf{r} - \mathbf{r}'|)} = \langle e^{-H_I^{(2)}(|\mathbf{r} - \mathbf{r}'|)} \rangle , \quad (\text{B10})$$

where the average is computed by means of the partition function in Eq. (B8), perturbatively expanded in powers of the fugacity y_0 .

We compute the first correction of order y_0^2 that corresponds to the effect on the external charges located at \mathbf{r} and \mathbf{r}' , of two additional internal charges located at \mathbf{s} and \mathbf{s}' and eventually we shall integrate over \mathbf{s} and \mathbf{s}' , in order to sum over all possible spatial configurations of these additional charges. It is assumed that the primed coordinates have negative charges, while the unprimed are positive. To order $O(y_0^2)$:

$$\begin{aligned} e^{-H_{eff}^{(2)}(|\mathbf{r} - \mathbf{r}'|)} &= e^{-H_I^{(2)}(|\mathbf{r} - \mathbf{r}'|)} \frac{\left\{ 1 + y_0^2 \int d^4 \mathbf{s} \int d^4 \mathbf{s}' e^{-2\pi^2 \mathcal{K} \ln |\mathbf{s} - \mathbf{s}'| + 2\pi^2 \mathcal{K} D(\mathbf{r}, \mathbf{r}', \mathbf{s}, \mathbf{s}') + O(y_0^4)} \right\}}{\left\{ 1 + y_0^2 \int d^4 \mathbf{s} \int d^4 \mathbf{s}' e^{-2\pi^2 \mathcal{K} \ln |\mathbf{s} - \mathbf{s}'| + O(y_0^4)} \right\}} = \\ &e^{-H_I^{(2)}(|\mathbf{r} - \mathbf{r}'|)} \left\{ 1 + y_0^2 \int d^4 \mathbf{s} \int d^4 \mathbf{s}' e^{-2\pi^2 \mathcal{K} \ln |\mathbf{s} - \mathbf{s}'|} \left[e^{2\pi^2 \mathcal{K} D(\mathbf{r}, \mathbf{r}', \mathbf{s}, \mathbf{s}') - 1} \right] + O(y_0^4) \right\} \end{aligned} \quad (\text{B11})$$

where the denominator provides the normalization factor and, as stated above, in the $O(y_0^2)$ correction in curly brackets, we discarded the $O(\mathcal{KT})$ part of $H_I^{(2)}$ and retained the $O(\mathcal{K})$ term only.

The interaction among the external and internal charges is contained in the factor $D(\mathbf{r}, \mathbf{r}', \mathbf{s}, \mathbf{s}') = \ln |\mathbf{r} - \mathbf{s}| - \ln |\mathbf{r} - \mathbf{s}'| - \ln |\mathbf{r}' - \mathbf{s}| + \ln |\mathbf{r}' - \mathbf{s}'|$, and the signs reflect the convention adopted for the primed and unprimed coordinates. It is convenient to change integration variables in Eq. (B11), from \mathbf{s}, \mathbf{s}' to $\mathbf{X} = (\mathbf{s} + \mathbf{s}')/2$, $\mathbf{x} = (\mathbf{s} - \mathbf{s}')$ and expand the term in square brackets in the second line of Eq. (B11) in powers of \mathbf{x} , as the factor in front of the square brackets, $e^{-2\pi^2\mathcal{K} \ln|\mathbf{x}|}$, disfavors largely separated pairs with $|\mathbf{x}| \gg 1$.

It is easy to check that $O(x^{2n})$ are exactly cancelled out in the expansion (note that ∇_i indicates the derivative with respect to the i -th component of the full argument of the related logarithm)

$$D(\mathbf{r}, \mathbf{r}', \mathbf{X}, \mathbf{x}) = \ln \left| \mathbf{r} - \mathbf{X} - \frac{\mathbf{x}}{2} \right| - \ln \left| \mathbf{r} - \mathbf{X} + \frac{\mathbf{x}}{2} \right| - \ln \left| \mathbf{r}' - \mathbf{X} - \frac{\mathbf{x}}{2} \right| + \ln \left| \mathbf{r}' - \mathbf{X} + \frac{\mathbf{x}}{2} \right| \simeq$$

$$x_i \nabla_i \ln |\mathbf{r}' - \mathbf{X}| - x_i \nabla_i \ln |\mathbf{r} - \mathbf{X}| + \frac{x_i x_j x_k}{24} \nabla_{i,j,k}^3 \ln |\mathbf{r}' - \mathbf{X}| - \frac{x_i x_j x_k}{24} \nabla_{i,j,k}^3 \ln |\mathbf{r} - \mathbf{X}| + O(x^5) \quad (\text{B12})$$

We can neglect $O(x^5)$ as they produce derivatives of order larger than four and are unnecessary to our purpose. Therefore, due to the presence of only odd powers of x in Eq. (B12), we need to keep even powers of $D(\mathbf{r}, \mathbf{r}', \mathbf{X}, \mathbf{x})$ in Eq. (B11), as the odd powers vanish due to the $d^4\mathbf{x}$ integration:

$$\int d^4\mathbf{X} \int d^4\mathbf{x} e^{-2\pi^2\mathcal{K} \ln|\mathbf{x}|} \left[e^{2\pi^2\mathcal{K} D} - 1 \right] = \int d^4\mathbf{X} \int d^4\mathbf{x} e^{-2\pi^2\mathcal{K} \ln|\mathbf{x}|} \left[\sum_{m=1}^{\infty} \frac{(2\pi^2\mathcal{K} D)^{2m}}{(2m)!} \right]. \quad (\text{B13})$$

After neglecting $O(\mathcal{K}^4)$ and higher orders terms in \mathcal{K} , and neglecting as well terms with order of derivatives larger than four, we are left with the following $O(x^4)$ and $O(x^2)$ contributions from the $O(\mathcal{K}^2)$ term:

$$\left[e^{2\pi^2\mathcal{K} D} - 1 \right] \simeq 2\pi^4\mathcal{K}^2 \left[\left(x_i \nabla_i \ln |\mathbf{r}' - \mathbf{X}| - x_i \nabla_i \ln |\mathbf{r} - \mathbf{X}| \right)^2 + \right.$$

$$\left. 2 \left(x_l \nabla_l \ln |\mathbf{r}' - \mathbf{X}| - x_l \nabla_l \ln |\mathbf{r} - \mathbf{X}| \right) \left(\frac{x_i x_j x_k}{24} \nabla_{i,j,k}^3 \ln |\mathbf{r}' - \mathbf{X}| - \frac{x_i x_j x_k}{24} \nabla_{i,j,k}^3 \ln |\mathbf{r} - \mathbf{X}| \right) \right] \quad (\text{B14})$$

These terms can be integrated by parts and, after symmetrization of the integrands, we get

$$e^{-H_{eff}}(|\mathbf{r}-\mathbf{r}'|) = e^{-H_I^{(2)}(|\mathbf{r}-\mathbf{r}'|)} \left\{ 1 + y_0^2 \int d^4\mathbf{X} \int d^4\mathbf{x} e^{-2\pi^2\mathcal{K} \ln|\mathbf{x}|} \cdot \right.$$

$$\left[\frac{\pi^4\mathcal{K}^2 x^2}{2} \left(2 \ln |\mathbf{r}' - \mathbf{X}| \Delta \ln |\mathbf{r} - \mathbf{X}| - \ln |\mathbf{r}' - \mathbf{X}| \Delta \ln |\mathbf{r}' - \mathbf{X}| - \ln |\mathbf{r} - \mathbf{X}| \Delta \ln |\mathbf{r} - \mathbf{X}| \right) + \right.$$

$$\left. \frac{\pi^4\mathcal{K}^2 x^4}{48} \left(2 \ln |\mathbf{r}' - \mathbf{X}| \Delta^2 \ln |\mathbf{r} - \mathbf{X}| - \ln |\mathbf{r}' - \mathbf{X}| \Delta^2 \ln |\mathbf{r}' - \mathbf{X}| - \ln |\mathbf{r} - \mathbf{X}| \Delta^2 \ln |\mathbf{r} - \mathbf{X}| \right) \right] \left. \right\} \quad (\text{B15})$$

The Δ and Δ^2 applied to the logarithms can be solved with the help of the relations in (B5) and (B6). The Δ^2 generates a δ -function that simplifies the computation of the $d^4\mathbf{X}$ integral while the Δ produces a term with the same structure of the $O(\mathcal{KT})$ term in (B7), namely

$$e^{-H_{eff}} = e^{-H_I^{(2)}} \left\{ 1 + y_0^2 \pi^4 \mathcal{K}^2 \left[2 J_2 \int d^4\mathbf{X} \left(\frac{\ln |\mathbf{r}' - \mathbf{X}|}{(\mathbf{r} - \mathbf{X})^2} - \frac{\ln |\mathbf{X}|}{(\mathbf{X})^2} \right) - \frac{J_4}{24} (8\pi^2) \ln |\mathbf{r}' - \mathbf{r}| \right] \right\}, \quad (\text{B16})$$

where we defined $J_n = \int d^4\mathbf{x} x^n e^{-2\pi^2\mathcal{K} \ln|\mathbf{x}|}$. To order $O(y_0^2)$, the content of the curly brackets in Eq. (B16) is equivalent to a resummed exponential form and this yields the correction to $H_I^{(2)}$. We observe the correspondence of the the various contributions in square brackets of (B16) with those of $H_I^{(2)}$ in Eq. (B7). In particular, we notice that the integral independent of \mathbf{r} and \mathbf{r}' in Eq. (B16) corresponds

to the self-energy contribution that has to be reabsorbed in y_0^2 , while the contribution proportional to the integral in $d^4\mathbf{X}$ in (B16) gets summed to the analogous term from Eq. (B7), yielding

$$\left(-\frac{\mathcal{K}\mathcal{T}}{2} + 2J_2 y_0^2 \pi^4 \mathcal{K}^2 \right) \int d^4\mathbf{X} \frac{\ln|\mathbf{r}' - \mathbf{X}|}{(\mathbf{r} - \mathbf{X})^2}. \quad (\text{B17})$$

Clearly the whole contribution in Eq. (B17) vanishes for the particular choice of \mathcal{T} that sets to zero the sum of the two terms in brackets. This choice requires $\mathcal{T} \propto \mathcal{K}$, which justifies why we discarded $O(\mathcal{K}\mathcal{T})$ terms in Eq. (B7) when computing higher order corrections. In this case, the interaction hamiltonian is proportional to $\ln|\mathbf{r}' - \mathbf{r}|$ only and we get

$$e^{-H_{eff}^{(2)}} = e^{-(2\pi^2)\mathcal{K} \ln|\mathbf{r}-\mathbf{r}'|} e^{-\frac{\mathcal{K}^2}{3}\pi^6 J_4 y_0^2 \ln|\mathbf{r}-\mathbf{r}'|} \quad (\text{B18})$$

that, with the suitable parametrization of the hamiltonian density $H_{eff}^{(2)}$ in terms of the effective coupling \mathcal{K}_{eff} , $H_{eff}^{(2)} = (2\pi^2)\mathcal{K}_{eff} \ln|\mathbf{r} - \mathbf{r}'|$, produces the relation

$$\mathcal{K}_{eff} = \mathcal{K} + \frac{\mathcal{K}^2}{6} \pi^4 y_0^2 J_4 = \mathcal{K} + \frac{\mathcal{K}^2}{3} \pi^6 y_0^2 \int_1^\infty dx x^{7-2\pi^2\mathcal{K}}. \quad (\text{B19})$$

The lower limit of integration in Eq. (B19) is set by the minimum distance allowed between charges, which is equal to the lattice spacing or $x = 1$ as all lengths are expressed in units of the lattice spacing.

By inverting Eq. (B19) and neglecting higher orders in \mathcal{K} , we obtain

$$\mathcal{K}_{eff}^{-1} = \mathcal{K}^{-1} - \frac{\pi^6 y_0^2}{3} \int_1^\infty dx x^{7-2\pi^2\mathcal{K}}. \quad (\text{B20})$$

An RG transformation on the couplings \mathcal{K}^{-1} and y_0 is arranged by requiring the invariance of \mathcal{K}_{eff} in Eq. (B20) under a rescaling of the lattice spacing. This is achieved by splitting the integral in (B20) into one integral from 1 to $b > 1$ and a second integral from b to ∞ :

$$\mathcal{K}_{eff}^{-1} = \mathcal{K}^{-1} - \frac{\pi^6 y_0^2}{3} \left(\int_1^b dx x^{7-2\pi^2\mathcal{K}} + \int_b^\infty dx x^{7-2\pi^2\mathcal{K}} \right). \quad (\text{B21})$$

As a second step, we define a new b -dependent coupling $\tilde{\mathcal{K}}$

$$\tilde{\mathcal{K}}^{-1} = \mathcal{K}^{-1} - \frac{\pi^6 y_0^2}{3} \int_1^b dx x^{7-2\pi^2\mathcal{K}} \quad (\text{B22})$$

and, after rescaling $x \rightarrow b\hat{x}$ in the second integral of Eq. (B20) so that the integral in $d\hat{x}$ goes from 1 to ∞ , we define the coupling \tilde{y}_0 containing all the b -dependence that appears after the x rescaling:

$$\tilde{y}_0^2 = y_0^2 b^{8-2\pi^2\mathcal{K}}. \quad (\text{B23})$$

These definitions allow us to rewrite the right hand side of Eq. (B20) in the same form, but with \mathcal{K} and y_0 replaced by $\tilde{\mathcal{K}}$ and \tilde{y}_0 , while leaving \mathcal{K}_{eff} unchanged in the left-hand side (more precisely, this procedure does not yield the replacement of \mathcal{K} in the exponent of x in Eq. (B20), although the latter substitution is admissible if we neglect higher orders of \mathcal{K} in the exponent). Therefore Eqs. (B22) and (B23) are the sought-after RG transformations that can be easily put in differential form:

$$b \frac{\partial \tilde{\mathcal{K}}^{-1}}{\partial b} = -\frac{\pi^6}{3} \tilde{y}_0^2 \quad ; \quad b \frac{\partial \tilde{y}_0}{\partial b} = \tilde{y}_0 \left(4 - \frac{\pi^2}{\tilde{\mathcal{K}}^{-1}} \right). \quad (\text{B24})$$

The flow equations in Eq. (B24) presents the same structure of the flow observed in Eqs. (16) and (17), at least by neglecting higher order in the couplings, provided one suitably relates $\tilde{\mathcal{K}}^{-1}$ and \tilde{y}_0 respectively to u_k and \tilde{g}_k . In particular the negative sign in the right hand side of the flow equation of $\tilde{\mathcal{K}}^{-1}$ is confirmed.

2. The general d-dimensional case

The same approach illustrated so far in this Appendix, when applied the BKT transition in $d = 2$, as it was originally formulated in [63], turns out to be even simpler, as the interaction hamiltonian density of Eq. (B7), in this case reduces to

$$H_{2d}^{(2)} = H_{core} + 2\pi K \ln |\mathbf{r} - \mathbf{r}'| \quad (\text{B25})$$

and the Green's function of the Laplacian in $d = 2$ is

$$\Delta \ln |\mathbf{r} - \mathbf{X}| = 2\pi \delta^2(\mathbf{r} - \mathbf{X}) . \quad (\text{B26})$$

By implementing the above changes in the procedure followed in the previous section, and in particular by retaining only the 2-derivative contribution in the computation of the corrections, which is relevant in $d = 2$, we arrive at the flow equations

$$b \frac{\partial \tilde{K}^{-1}}{\partial b} = 4\pi^3 \tilde{y}_0^2 \quad ; \quad b \frac{\partial \tilde{y}_0}{\partial b} = \tilde{y}_0 \left(2 - \frac{\pi}{\tilde{K}^{-1}} \right) , \quad (\text{B27})$$

which display a positive right-hand side in the flow equation of \tilde{K}^{-1} . This switching of sign between Eqs. (B24) and (B27) can be traced back to the change of sign between Eqs. (B6) and (B26) that are used respectively in $d = 4$ and in $d = 2$.

Therefore, the essential difference observable on the flow of the couplings when the number of dimensions of the system is changed, is essentially due to the different sign coming from the application of the suitable power of the Laplacian to the logarithmic function.

This argument can be generalized to generic even dimension d . In fact, in this case the approach discussed so far in $d = 4$ and in $d = 2$ is recovered by considering the following hamiltonian density

$$H = \int d^d x \nabla_i^{d/2} \theta \nabla_i^{d/2} \theta \quad (\text{B28})$$

and the essential point is that after integrating by parts we end up with the computation of $\Delta^{d/2} \ln |\mathbf{X} - \mathbf{r}|$, which provides different signs depending on d ,

$$\Delta^{\frac{d}{2}} \ln |\mathbf{X} - \mathbf{r}| = (-1)^{\frac{d}{2}+1} \alpha_d^2 \delta^d(|\mathbf{X} - \mathbf{r}|) , \quad (\text{B29})$$

where α_d^2 is a positive constant. Then, the sign of the right hand side of Eq. (B29) is directly related to the sign of the coefficient already determined in the right hand side of the first flow equation in Eq. (B24) and in Eq. (B27). Accordingly, in general the sign of the corresponding flow in d dimensions changes as $(-1)^{\frac{d}{2}+1}$.

The origin of the sign in Eq. (B29) can be traced back to the specific form of the Laplacian Green's function for $d > 2$ (the $d = 2$ case is in Eq. (B26)), reported in [75] (here β_d^2 is a positive constant),

$$\Delta \frac{1}{|\mathbf{X} - \mathbf{r}|^{d-2}} = -\beta_d^2 \delta^d(|\mathbf{X} - \mathbf{r}|) . \quad (\text{B30})$$

Indeed, if we now rename the Green's function

$$\mathcal{S}_d(\mathbf{s}_1, \mathbf{s}_2) = \frac{1}{|\mathbf{s}_1 - \mathbf{s}_2|^{d-2}} \quad (\text{B31})$$

and define the following convolution

$$\mathcal{C}_d(\mathbf{X}, \mathbf{r}) = \left(\prod_{k=1}^{\frac{d}{2}-1} \int d^d s_k \right) \mathcal{S}_d(\mathbf{X}, \mathbf{s}_1) \left(\prod_{j=1}^{\frac{d}{2}-2} \mathcal{S}_d(\mathbf{s}_j, \mathbf{s}_{j+1}) \right) \mathcal{S}_d(\mathbf{s}_{\frac{d}{2}-1}, \mathbf{r}) , \quad (\text{B32})$$

with the help of Eqs. (B30) and (B31), it is easy to verify that:

$$\Delta^{\frac{d}{2}} \mathcal{C}_d(\mathbf{X}, \mathbf{r}) = (-\beta_d^2)^{\frac{d}{2}} \delta^d(|\mathbf{X} - \mathbf{r}|) \quad (\text{B33})$$

and also, by direct inspection, to check the following relation (γ_d^2 is a positive constant),

$$C_d(\mathbf{X}, \mathbf{r}) = -\gamma_d^2 \ln \frac{|\mathbf{X} - \mathbf{r}|}{R}. \quad (\text{B34})$$

Combining Eqs. (B33) and (B34), we obtain the desired sign prescription in Eq. (B29) and conclude that the sign in Eq. (16) (or the first equation in Eq. (B27)), is a consequence of the dimensionality of the system.

-
- [1] W. Thirring, *Phys. Rev.* **77**, 570 (1950).
 - [2] A. Pais and G. E. Uhlenbeck, *Phys. Rev.* **79**, 145 (1950).
 - [3] K. S. Stelle, *Phys. Rev.* **D 16**, 953 (1977).
 - [4] F. J. de Urries and J. Julve, *J. Phys.* **A 31**, 6949 (1998). [arXiv:hep-th/9802115](#).
 - [5] S. W. Hawking and T. Hertog, *Phys. Rev.* **D 65**, 103515 (2002). [arXiv:hep-th/0107088](#).
 - [6] J. Collins, A. Perez, D. Sudarsky, L. Urrutia, H. Vucetich, *Phys. Rev. Lett.* **93**, 191301 (2004). [arXiv:gr-qc/0403053](#).
 - [7] R. P. Woodard, *Lect. Notes Phys.* **720**, 403 (2007). [astro-ph/0601672](#).
 - [8] P. Hořava, *Phys. Rev.* **D 79**, 084008 (2009). [arXiv:0901.3775](#).
 - [9] P. Hořava, *Phys. Rev. Lett.* **102**, (2009) 161301. [arXiv:0902.3657](#).
 - [10] A.O. Barvinsky, D. Blas, M. Herrero-Valea, S.M. Sibiryakov, C.F. Steinwachs, *Phys. Rev.* **D 93**, 064022 (2016). [arXiv:1512.02250](#).
 - [11] A.O. Barvinsky, D. Blas, M. Herrero-Valea, S.M. Sibiryakov, C.F. Steinwachs, *Phys. Rev. Lett.* **119**, 211301 (2017). [arXiv:1706.06809](#).
 - [12] A.O. Barvinsky, D. Blas, M. Herrero-Valea, S.M. Sibiryakov, *Phys. Rev.* **D 100**, 026012 (2019). [arXiv:1905.03798](#).
 - [13] A.O. Barvinsky, A.V. Kurov, S.M. Sibiryakov, *Phys. Rev.* **D 105**, 044009 (2022). [arXiv:2110.14688](#).
 - [14] D. Anselmi and M. Halat, *Phys. Rev.* **D 76**, 125011 (2007). [arXiv:0707.2480](#).
 - [15] R. Iengo, J. G. Russo, and M. Serone, *JHEP* **11**, 020 (2009). [arXiv:0906.3477](#).
 - [16] A. Dhar, G. Mandal, and S. R. Wadia, *Phys. Rev.* **D 80**, 105018 (2009). [arXiv:0905.2928](#).
 - [17] P. Horava, *Phys. Lett.* **B 694**, 172 (2011). [arXiv:0811.2217](#).
 - [18] M. Eune, W. Kim, and E. J. Son, *Phys. Lett.* **B 703**, 100 (2011). [arXiv:1105.5194](#).
 - [19] J. Alexandre, *Int. J. Mod. Phys. A* **26**, 4523 (2011). [arXiv:1109.5629](#).
 - [20] K. Kikuchi, *Prog. Theor. Phys.* **127**, 409 (2012). [arXiv:1111.6075](#).
 - [21] W. Chao, *Commun. Theor. Phys.* **65**, 743 (2016). [arXiv:0911.4709](#).
 - [22] A. R. Solomon and M. Trodden, *JCAP* **02**, 031 (2018). [arXiv:1709.09695](#).
 - [23] D. Zappalà, *Eur. Phys. J.* **C 82**, 341, (2022). [arXiv:2111.08385](#).
 - [24] E. Rizza and D. Zappalà, *Mod. Phys. Lett.* **A 37**, 2250203, (2022). [arXiv:2209.11060](#).
 - [25] B. Chen, Q.G. Huang, *Phys. Lett.* **B 683**, 108 (2010).
 - [26] J. Ellis, R. Konoplich, N. E. Mavromatos, L. Nguyen, A. S. Sakharov, and E. K. Sarkisyan-Grinbaum, *Phys. Rev.* **D 99**, 083009 (2019). [arXiv:1807.00189](#).
 - [27] R. M. Hornreich, M. Luban, S. Shtrikman, *Phys. Rev. Lett.* **35**, 1678 (1975).
 - [28] A. Erzan, G. Stell, *Phys. Rev.* **B 16**, 4146 (1977).
 - [29] J. Sak, G. S. Grest, *Phys. Rev.* **B 17**, 3602 (1978).
 - [30] R. M. Hornreich, *Journal of Magnetism and Magnetic Materials* **15**, 387 (1980).
 - [31] H. Diehl and M. Shpot, *J. Phys.* **A35**, 6249 (2002). [arXiv:cond-mat/0204267](#).
 - [32] R. Anglani, R. Casalbuoni, M. Ciminale, N. Ippolito, R. Gatto, M. Mannarelli, M. Ruggieri, *Rev. Mod. Phys.* **86** 509 (2014). [arXiv:1302.4264](#).
 - [33] P. Castorina, G. Nardulli and D. Zappalà, *Phys. Rev.* **D 72**, 076006 (2005). [arXiv:hep-ph/0505089](#).
 - [34] M. Buballa, S. Carignano, *Prog. Part. Nucl. Phys.* **81**, 39 (2015). [arXiv:1406.1367](#).
 - [35] R. D. Pisarski, V. V. Skokov, A. M. Tsvetik, *Phys. Rev.* **D 99**, 074025 (2019). [arXiv:1801.08156](#).
 - [36] R. D. Pisarski, A. M. Tsvetik, S. Valgushev, *Phys. Rev.* **D 102**, 016015 (2020). [arXiv:2005.10259](#).
 - [37] A. Bonanno and D. Zappalà, *Nucl. Phys.* **B 893**, 501 (2015). [arXiv:1412.7046](#).
 - [38] D. Zappalà, *Phys. Lett.* **B 773**, 213 (2017). [arXiv:1703.00791](#).
 - [39] D. Zappalà, *Phys. Rev.* **D 98**, 085005 (2018). [arXiv:1806.00043](#).
 - [40] C. Wetterich, *Phys. Lett.* **B 301**, 90 (1993). [arXiv:1710.05815 \[hep-th\]](#).
 - [41] T. R. Morris, *Int. J. Mod. Phys.* **A 9**, 2411 (1994). [arXiv:hep-ph/9308265](#).
 - [42] J. Berges, N. Tetradis, C. Wetterich, *Phys. Rept.* **363**, 223 (2002). [arXiv:hep-ph/0005122](#).
 - [43] A. Codello, N. Defenu, G. D’Odorico, *Phys. Rev.* **D 91**, 105003 (2015). [arXiv:1410.3308](#).
 - [44] N. Defenu, A. Trombettoni, A. Codello, *Phys. Rev.* **E 92**, 289 (2015). [arXiv:1409.8322](#).

- [45] N. Defenu, A. Codello, *Phys. Rev. D* **98**, 016013 (2018). [arXiv: 1711.01809](#).
- [46] M. Gräter, C. Wetterich, *Phys. Rev. Lett.* **75**, 378 (1995). [arXiv:hep-ph/9409459](#).
- [47] P. Jakubczyk, W. Metzner, *Phys. Rev. B* **95**, 085113 (2017). [arXiv: 1606.04547](#).
- [48] P. Jakubczyk, N. Dupuis, B. Delamotte, *Phys. Rev. E* **90**, 062105 (2014). [arXiv:1409.1374](#).
- [49] N. Defenu, A. Trombettoni, I. Nándori, T. Enss, *Phys. Rev. B* **96**, 174505 (2017). [arXiv:1706.00618](#).
- [50] J. Krieg and P. Kopietz *Phys. Rev. E* **96**, 042107 (2017). [arXiv: 1707.01098](#).
- [51] I. Nándori, J. Polonyi, K. Sailer, *Phys. Rev. D* **63**, 045022 (2001). [arXiv:hep-th/9910167](#).
- [52] S. Nagy, I. Nándori, J. Polonyi, K. Sailer, *Phys. Rev. Lett.* **102**, 241603 (2009). [arXiv:0904.3689](#).
- [53] I. Nándori, S. Nagy, K. Sailer, A. Trombettoni, *Phys. Rev. D* **80**, 025008 (2009). [arXiv:0903.5524](#).
- [54] R. Daviet, and N. Dupuis, *Phys. Rev. Lett.* **122**, 155301 (2019). [arXiv:1812.01908](#).
- [55] P. Jentsch, R. Daviet, N. Dupuis and S. Floerchinger, *Phys. Rev. D* **105**, 016028 (2022). [arXiv:2106.08310](#).
- [56] I. Nándori, *Nucl. Phys. B* **975**, 115681 (2022). [arXiv:1108.4643](#).
- [57] D. Zappalà, *Int. J. Geom. Meth. Mod. Phys.* **17**, 2050053 (2020). [arXiv:1912.03071](#).
- [58] N. Defenu, A. Trombettoni, and D. Zappalà, *Nucl. Phys. B* **964**, 115295 (2021). [arXiv:2003.04909](#).
- [59] P. Minnhagen, *Rev. Mod. Phys.* **59**, 1001 (1987).
- [60] V.L. Berezinskii, *Sov. Phys. JETP* **32**, 493 (1971).
- [61] J. M. Kosterlitz, D. J. Thouless, *J. Phys. C* **5**, L124 (1972).
- [62] J. M. Kosterlitz, D. J. Thouless, *J. Phys. C* **6**, 1181 (1973).
- [63] J. V. José, L. P. Kadanoff, S. Kirkpatrick, D. R. Nelson, *Phys. Rev. B* **16**, 1217 (1977).
- [64] A.L. Fetter and J.D. Walecka, *Quantum Theory of Many-Particle Systems*, McGraw-Hill, Boston, (1971).
- [65] A. Bonanno, D. Zappalà, *Phys. Lett. B* **504**, 181 (2001). [arXiv:hep-th/0010095](#). β
- [66] D. Buccio and R. Percacci, *JHEP* **10**,113 (2022). [arXiv:2207.10596](#).
- [67] Martin Reuter, *Phys. Rev. D* **57**, 971 (1998). [arXiv:hep-th/9605030](#).
- [68] Martin Reuter, Holger Weyer, *Phys. Rev. D* **79**, 105005 (2009). [arXiv:0804.1475](#).
- [69] Martin Reuter, Holger Weyer, *Phys. Rev. D* **80**, 025001 (2009). [arXiv:0804.1475](#).
- [70] Pedro F. Machado, R. Percacci, *Phys. Rev. D* **80**, 024020 (2009). [arXiv:0904.2510](#).
- [71] Alfio Bonanno, Martin Reuter, *Phys. Rev. D* **87**, 084019 (2013). [arXiv:1302.2928](#).
- [72] Juergen A.Dietz, Tim R. Morris, Zoe H. Slade, *Phys. Rev. D* **94** 124014 (2016). [arXiv:1605.07636](#).
- [73] Alfio Bonanno, Maria Conti, Dario Zappalà, *Phys. Lett. B* **847**, 138311 (2023). [arXiv:2309.15514](#).
- [74] I.S. Gradshteyn, I.M. Ryzhik, *Table of Integrals, Series, and Products*. 7th Edition, Academic Press, (2007).
- [75] L. Evans, *Partial Differential Equations, Second Edition*, Graduate studies in Mathematics, American Mathematical Society, Providence RI, (2010).